MODEL STUDY OF REACTOR CONTAINMENT SUMP FLOW CHARACTERISTICS VIRGIL C. SUMMER NUCLEAR GENERATING STATION

by
James B. Nystrom

Research Sponsored by
South Carolina Electric and Gas Company

ALDEN RESEARCH LABORATORY
WORCESTER POLYTECHNIC INSTITUTE

47-81/M260EF

July 1981

MODEL STUDY OF REACTOR CONTAINMENT SUMP FLOW CHARACTERISTICS

VIRGIL C. SUMMER NUCLEAR GENERATING STATION

by

James B. Nystrom

Research Sponsored by

South Carolina Electric and Gas Company

George E. Hecker, Director

ALDEN RESEARCH LABORATORY

WORCESTER POLYTECHNIC INSTITUTE

HOLDEN, MASSACHUSETTS

June 1981

ABSTRACT

A hydraulic model of the containment building sump for the Virgil C. Summer Nuclear Generating Station was constructed at a scale of 1:2.93. Residual heat removal pumps and reactor building spray pumps withdraw water from the sump after a postulated loss of coolant accident for re-injection into the core and building. To assure acceptable operation of the pumps, the model was tested for a wide range of possible approach flow distributions, floor grating blockage schemes, and screen blockage schemes. The tests were designed to assure that no air entraining vortices were formed, head losses across the screens and in the inlet were acceptable, and swirl in the pump suction pipes was acceptable.

The maximum vortex activity noted was a surface dimple, which originated as a vortex shed from obstructions in the approach flow and was carried across the sump by the approach flow.

Test results indicated that the maximum swirl angle was 9.5 degrees, while average swirl angle was about 3 degrees. For an RHR flowrate of 4500 gpm per line, loss measurements indicated an average pipe inlet loss of 0.37 ft and screen losses ranging from 0.05 ft for clean screens to 0.19 ft for the worst case of 50 percent blockage. The reactor building spray lines had flowrates of 3000 gpm, which reduced pipe inlet losses to 0.30 ft and screen losses to 0.12 ft maximum.

TABLE OF CONTENTS

INTRODUCTION

The reactor containment building of the Virgil C. Summer Generating Station is provided with both a residual heat removal (RHR) system designed to cool the shutdown reactor core and a reactor building (RB) spray system to cool the containment building, both systems to operate only in the event of a Loss of Coolant Accident (LOCA). Initially, water for these systems is drawn from the refueling water storage tank. When the water level in this tank reaches a predetermined level, the residual heat removal system is switched from the injection mode to the recirculation mode. At this point, water is drawn from the containment sump, which then contains water drained from the break and from the containment spray system. Flow approaching the sump is affected by the geometry of the flow path including various appurtenant structures and equipment. Water level, pump discharge, and water temperature could vary during the recirculation mode, which lasts for an extended period to provide sufficient heat removal.

The Alden Research Laboratory (ARL) of Worcester Polytechnic Institute (WPI) was authorized by South Carolina Electric and Gas Company to construct and test a model of the Virgil C. Summer Nuclear Generating Station containment sump with the object of investigating free surface vortex formation, swirl in the inlet piping, inlet losses, or any other flow conditions that could adversely affect the performance of the residual heat removal pumps and the reactor building spray pumps in the recirculation mode. Operating conditions involving a wide range of possible approach flow distributions, floor grating blockages, screen blockages (due to debris), and combinations thereof were tested in the model.

This report presents the findings of the study and includes a description of the prototype and the model, and summarizes conditions investigated, similitude considerations, test procedures, instrumentation, and interpretation of results.

PROTOTYPE DESCRIPTION

Both the RHR and the RB spray systems have a pair of pumps and sumps to maintain independent redundant systems. An RHR sump and an RB spray sump are located in each of two containment sumps which are located in the reactor building floor at elevation 412 ft between the bioshield wall and the containment wall, as shown in Figure 1. The bioshield wall protects the sumps from direct impingement of possible breakflow jets. Each containment sump contains two sets of fine screens and two pump sumps from which the pump suction line exits. The shallow containment sumps are approximately trapezoidal in shape, about 22 ft by 10 ft in plan, and are 4 ft deep. A 4 ft wide wall extending 3 ft high from the containment sump floor separates the RHR and RB spray pump sumps. A 6 inch high curb surrounds the containment sumps and standard floor grates cover the sump area at floor elevation.

Within the shallow containment sumps, two 4 ft square pump sumps descend 8 ft to elevation 400 ft. The cross-section of the pump sumps, Figure 2, shows the pump suction lines exiting the sumps approximately horizontally with initial centerline elevation 402 ft. The RHR and RB spray pump suction lines have diameters of 14 and 12 inches, respectively. Quasi-bellmouths consisting of standard reducers and flanges are used on both inlets. The inlet piping to the pumps extends at a shallow slope about 56 ft to an isolation valve prior to the pump.

Two sets of vertical screens protect each pump sump from ingestion of debris into the pump systems. An outer screen, shown in Figure 3, is 6 ft square in plan and extends from the bottom of the containment sump, elevation 408 ft, about two feet to elevation 410 ft. A solid cover extends from elevation 410 ft to elevation 412 ft, the grating level, and a horizontal solid plate covers the outer screen. The outer screen has 1/2 inch mesh. The inner screen, Figure 2, has the dimensions of the pump sump, 4 ft square, and has 1/4 inch mesh. The inner screen extends from elevation 410 ft to elevation 411 ft 11 inches. A solid plate is located from elevation 408 ft to elevation 410 ft. The horizontal cover has access doors, and a ladder provides access to the pump sump.

In the recirculation mode, after a postulated LOCA, water approaches the sumps laterally through the annulus created by the bioshield wall and the containment wall. A secondary flow path is from the next level above the sump. The RB spray flow may collect on the upper floor, which has a 6 inch high curb surrounding all openings except a stairwell near the southwest sump. Assuming the floor drains are completely blocked, the stairwell provides the only flow path for the RB spray collected at that level.

Minimum water level for recirculation mode is elevation [redacted] 417 ft. Runout flowrates for the RHR and RB spray pumps are 4500 gpm per line and 3000 gpm per line, respectively.

A site visit was conducted to assure the interpretation and completeness of drawings in regard to the primary approach flow paths, possible secondary approach flow paths, and various equipment obstructing the flow paths.

Various equipment, located at elevation 412 ft, with diameters greater than 3 inches were considered relevant in influencing flow conditions and these are shown in Figure 6. The main pieces of relevant equipment are the accumulator and its pipeline, an RHR pipe loop and valve, auxiliary piping over the southwest sump, a fan, lubrication lines, support columns, and instrument cabinets. Photographic documentation during the site visit allowed details to be checked as model design and construction proceeded. Photographs 1 and 2 show the areas in the prototype surrounding the West and Southwest sumps during construction, when temporary scaffolding was in place.

SIMILITUDE

The study of dynamically similar fluid motions forms the basis for the design of models and the interpretation of experimental data. The basic concept of dynamic similarity may be stated as the requirement that two systems with geometrically similar boundaries have geometrically similar flow patterns at corresponding instants of time (3). Thus, all individual forces acting on corresponding fluid elements of mass must have the same ratios in the two systems.

The condition required for complete similitude may be developed from Newton's second law of motion:

$$F_i = F_p + F_g + F_v + F_t \qquad (1)$$

where

F_i = inertia force, defined as mass, M, times the acceleration, a

F_p = pressure force connected with or resulting from the motion

F_g = gravitational force

F_v = viscous force

F_t = force due to surface tension

Additional forces may be relevant under special circumstances, such as fluid compression, magnetic or Corriolis forces, but these had no influence on this study and were, therefore, not considered in the following development.

Two systems which are geometrically similar are dynamically similar if both satisfy the dimensionless form of the equation of motion. Equation (1) can be made dimensionless by dividing all the terms by F_i. Rewriting each of the forces of Equation (1) as:

F_p = net pressure x area = $\alpha_1 \Delta p L^2$

F_g = specific weight x volume = $\alpha_2 \gamma L^3$

F_v = shear stress x area = $\alpha_3 \mu \Delta u/\Delta y$ x area = $\alpha_3 \mu u L$

F_t = surface tension x length = $\alpha_4 \sigma L$

F_i = density x volume x acceleration = $\alpha_5 \rho L^3 u^2/L = \alpha_5 \rho u^2 L^2$

where

α_1, α_2, etc. = proportionality factors

L = representative linear dimension

p = net pressure

γ = specific weight

μ = dynamic viscosity

σ = surface tension

ρ = density

u = representative velocity

Substituting the above terms in Equation (1) and making it dimensionless by dividing by the inertial force, F_i, we obtain

$$\frac{\alpha_1}{\alpha_5} E^{-2} + \frac{\alpha_2}{\alpha_5} F^{-2} + \frac{\alpha_3}{\alpha_5} R^{-1} + \frac{\alpha_4}{\alpha_5} W^{-2} = 1 \qquad (2)$$

where

$$E = \frac{u}{\sqrt{\Delta p/\rho}} = \text{Euler number;} \quad \frac{\text{Inertia Force}}{\text{Pressure Force}}$$

$$F = \frac{u}{\sqrt{gL}} = \text{Froude number;} \quad \frac{\text{Inertia Force}}{\text{Gravity Force}}$$

$$R = \frac{u\,L}{\mu/\rho} = \text{Reynolds number;} \quad \frac{\text{Inertia Force}}{\text{Viscous Force}}$$

$$W = \frac{u}{\sqrt{\sigma/\rho L}} = \text{Weber number;} \quad \frac{\text{Inertia Force}}{\text{Surface Tension Force}}$$

Since the proportionality factors, α_i, are the same in model and prototype, complete dynamic similarity is achieved if all the dimensionless groups, E, F, R, and W, have the same values in model and prototype. In practice, this is difficult to achieve. For example, to have the values of F and R the same requires either a 1:1 "model" or a fluid of very low kinematic viscosity in the reduced scale model. Hence, the accepted approach is to select the predominant forces and design the model according to the appropriate dimensionless group. The influence of the other forces would be secondary and are called scale effects (2, 3).

Froude Scaling

Models involving a free surface are constructed and operated using Froude similarity since the flow process is controlled by gravity and inertia forces. The Froude number, representing the ratio of inertia to gravitational force,

$$F = u/\sqrt{gs} \qquad (3)$$

where

u = average velocity in the pipe

g = gravitational acceleration

s = submergence, the representative linear dimension

was, therefore, made equal in model and prototype.

$$F_r = F_m/F_p = 1 \qquad (4)$$

where m, p, and r denote model, prototype, and ratio between model and prototype, respectively.

In modeling of an intake sump to study the formation of vortices, it is important to select a reasonably large geometric scale to achieve large Reynolds numbers and to reproduce the curved flow pattern in the vicinity of the intake (4). At sufficiently high Reynolds number, an asymptotic behavior of energy loss coefficients with Reynolds number is usually observed (2). Hence, with $F_r = 1$, the basic Froudian scaling criterion, the Euler numbers, E, will be equal in model and prototype. This implies that flow patterns and loss coefficients are equal in model and prototype at sufficiently high Reynolds numbers. A geometric scale of $L_r = L_m/L_p = 1/2.93$ was chosen for the model, where L refers to length. From Equations (3) and (4), using $s_r = L_r$, the velocity, discharge, and time scales were:

$$u_r = L_r^{0.5} = 1/\sqrt{2.93} = \frac{1}{1.71} \qquad (5)$$

$$Q_r = L_r^2 u_r = L_r^{2.5} = 1/(2.93)^{2.5} = \frac{1}{14.66} \qquad (6)$$

$$t_r = L_r^{0.5} = 1/\sqrt{2.93} = \frac{1}{1.71} \qquad (7)$$

Similarity of Vortex Motion

Fluid motions involving vortex formation in sumps of low head pump intakes have been studied by several investigators (1, 4, 5, 6).

Viscous and surface tension forces could influence the formation and strength of vortices (1, 5). The relative magnitude of these forces on the fluid inertia force is reflected in the Reynolds and Weber numbers, respectively, which are defined as:

$$R = u\, d/\nu \tag{8}$$

$$W = \frac{u}{(\sigma/\rho r)^{1/2}} \tag{9}$$

where r = characteristic radius of vortex and d = intake diameter. It was important for this study to ascertain any deviations in similitude attributable to viscous and surface tension forces in the interpretation of model results. For large R and W, the effects of viscous and surface tension are minimal, i.e., inertial forces predominate. Surface tension effects are negligible when r is large, which will be true for weak vortices where the free surface is essentially flat. Conversely, only strong air core vortices are subject to surface tension scale effects. Moreover, an investigation using liquids of the same viscosity but different surface tension coefficients ($\sigma = 4.9 \times 10^{-3}$ lb/ft to 1.6×10^{-3} lb/ft) showed practically no effect of surface tension forces on the vortex flow (1). The vortex severity, S, is therefore mainly a function of the Froude number, but could also be influenced by the Reynolds number.

$$S = S\,(F, R) \tag{10}$$

Anwar (4) has shown by principles of dimensional analysis that the dynamic similarity of fluid motion in an intake is governed by the dimensionless parameters given by

$$\frac{4Q}{u_\theta a^2}, \quad \frac{u}{\sqrt{2gs}}, \quad \frac{Q}{\nu s}, \text{ and } \frac{d}{2s}$$

where

Q = discharge through the outlet

u_θ = tangential velocity at a radius equal to that of outlet pipe

d = diameter of the outlet pipe

Surface tension effects were neglected in his analysis, being negligible for weak vortices. The influence of viscous effects was defined by the parameter $Q/(\nu\ s)$, known as a radial Reynolds number, R_R.

For similarity between the dimensions of a vortex of strengths up to and including a narrow air-core type, it was shown that the influence of R_R becomes negligible if $Q/(\nu\ s)$ was greater than 3×10^4 (4). As strong air-core type vortices, if present in the model, would have to be eliminated by modified sump design, the main concern for interpretation of prototype performance based on the model performance would be on the similarity of weaker vortices, such as surface dimples and dye-cores. For the prototype of the present study, the values of R_R for the operating temperature ranges of 70° and above, and using the submergence to the floor grating, was greater than 1.1×10^5. In the model, the value of R_R for the RHR sumps was 2.6×10^4 for Froude velocity and 4.4×10^4 for prototype velocity both for water temperatures of 50°F. Thus, viscous forces would have only a secondary role in the present study. Dynamic similarity is obtained by equalizing the parameters $4Q/u_\theta d^2$, $u/\sqrt{2gs}$, and $d/2s$ in model and prototype. A Froudian model would satisfy this condition.

To compensate for any possible excessive viscous energy dissipation and consequently less intense model vortex, various investigators have proposed increasing the model flow and, therefore, the approach and intake velocity, since the submergence is maintained constant. Operating the model at the prototype inlet velocity (pipe velocity) is believed by some researchers to achieve the desired results (1). This is often referred to as Equal Velocity Rule, and is considered to give conservative predictions of prototype performance. The test procedure for the present study incorporated testing the model at prototype pipe velocities to achieve conservative predictions.

ARL Vortex Activity Projection Technique

ARL has conducted an extensive research program to assure that the conclusions regarding the effect of Reynolds number on vortex activity in the model are valid for the prototype. A technique of extrapolating model vortex activity to prototype Reynolds numbers (17) by using elevated model water temperatures and varying model flow velocity (Froude ratio) has been applied to several studies (7, 12, 18, 19, 29). Figure 4 illustrates the method used to investigate scale effects and predict vortex types in the prototype based on model results (7). The ordinate, F_r, is the ratio of model to prototype Froude number, while the abscissa is the inlet pipe Reynolds number, R. The objective is to determine flow conditions at $F_R = 1$ at prototype R from tests at lower than prototype R. Assume the model to operate at flow less than Froude scaling ($F_r < 1$) at point a_1. By increasing the discharge in the model while keeping the same submergence and temperature, F_r and R are increased corresponding to a point, a_N, where a vortex of type N was first observed. The model Reynolds number can also be changed by varying the kinematic viscosity with temperature changes, and similar tests performed to locate b_N, another point on the locus of type N vortices. Extrapolation of the line of constant vortex strength of type N can be made to a prototype Reynolds number at the proper Froude number ($F_r = 1$), point p_N. The locus could represent any expedient measure of vortex severity. Any scale effects due to viscous forces would be evaluated and taken into account by such a projection procedure. The high temperature-high flow tests were used in the similar fashion for projecting the inlet loss coefficients (from the pressure gradient measurements) and the swirl severities (from vortimeter readings) over a wide range of Reynolds and Froude numbers.

Experience has shown that incoherent swirling flow is even less dependent on Reynolds number than a coherent vortex core. Eliminating the tendency for coherent vortices axiomatically removes possible scale effects. In reactor sumps, the design criteria eliminate the possibility of coherent vortex cores in an acceptable design.

Figure 5 shows the results of one recirculation sump model (19) which are typical of the other four studies conducted. As can be seen from the data, which are for the final design with vortex suppressor grids, there are no measurable changes in vortex strength with Reynolds number. This is reasonable since the Reynolds numbers are all above the limiting value (1, 4), a previously described similitude requirement. Minor increases in vortex strength occur when the Froude ratio is increased. Other measurements, such as swirl in the inlet pipe, have also shown no measurable dependence on Reynolds number. This indicates that reduced scale model tests are a direct indication of prototype performance for weak vortices, particularly if vortex suppressors are part of the design, even at Froude scaled flow (i.e., $F_r = 1$). Tests at higher than Froude scaled flow are seen to give conservative results, i.e., somewhat stronger vortices than expected in the prototype. Since for this study the minimum Reynolds number is comparable to the minimum for the previous studies which indicated no increase in vortex activity for increasing Reynolds numbers at constant Froude ratio, it is concluded that no scale effects will be present in the final design.

Dynamic Similarity of Flow Through Screens

In addition to providing protection from debris, screens tend to suppress non-uniformities of the approach flow. The aspects of flow through screens of concern in a model study are: (1) energy loss of fluid passing through the screen; (2) modification of velocity profile and the deflection of streamlines at the screen; and (3) production of turbulence. As all these factors could affect vortex formation in a sump with approach flow directed through screens, a proper modeling of screen parameters is important.

The loss of energy across the screen occurs at a rate proportional to the drop in pressure, and this loss dictates the effectiveness of the screen in altering velocity profiles. The pressure drop across the screen is analogous to the drag induced by a row of cylinders in a flow field and could be expressed in terms of a pressure-drop coefficient K (or alternately a drag coefficient), defined as (8),

$$K = \frac{\Delta p}{1/2\ \rho\ U^2} = \frac{\Delta H}{U^2/2g} \qquad (11)$$

where

Δp = drop in pressure across the screen

U = mean velocity of approach flow

ρ = density of the fluid

ΔH = head loss across the screen

g = acceleration due to gravity

From the available literature on the topic (8, 9, 10), it may be seen that

$$K = f(R_s, S', \text{Pattern}) \qquad (12)$$

where

R_s = screen Reynolds number, $U\ d_w/\nu$, d_w being the wire diameter of the screen

S' = solidity ratio, equal to the ratio of closed area to total area of screen

Pattern = geometry of the wire screen

If the solidity ratio and the wire mesh pattern are the same in the model and prototype screens, the corresponding values of K would only be a function of the screen Reynolds number. This is analogous to the coefficient of drag the case of the circular cylinder. It is known that K becomes practically independent of R_s at values of R_s greater than about 1000 (8, 11). However, for models with low approach flow velocity and with fine wire screens, it is necessary to ascertain the influence of R_s on K for both the model and prototype screens before selecting screens for the model which are to scale changes in velocity distribution.

Velocity modification equations relating the upstream velocity profile and downstream velocity profile have been derived based on different theories (8). Most of these indicate a linear relationship between upstream velocity profile and downstream velocity profile, shape and solidity ratio of screen, and value of K. If the wire shape and solidity ratios are the same in the model and prototype screens, it is possible to select a suitable wire diameter to keep the values of K approximately the same for the model and prototype screens at the corresponding Reynolds number ranges. Identical velocity modifications would be produced by the respective screens if the loss coefficients were identical.

The pressure loss coefficient to Reynolds number relationship of fine screens have been investigated at ARL (12). Based on the similarity of pressure loss and velocity modifications, an appropriate model screen was chosen, which had a loss coefficient within 10% of the predicted prototype loss coefficient. This was considered sufficient since actual losses and, therefore, velocity profile modifications, were small (about 0.05 ft) and screen blockages cause changes in velocity distributions far outweighing changes due to screen.

MODEL DESCRIPTION

The model was constructed to a geometric scale of 1:2.93 with boundaries, as indicated in Figure 1. Model boundaries were chosen at locations where flow pattern control in the prototype would be sufficiently removed from the sump areas to avoid boundary effects, especially once screen blockage is considered. Screen blockage has consistently generated the most severe vortices and swirl in the numerous past ECCS sump studies at ARL. The model was located in an existing elevated tank to provide access to observe flow patterns in the pump sumps. Photograph 3 is an overall view of the completed model. Inflow was provided from a sump beneath the model by a vertical pump, and the water level in the model was controlled by an adjustable weir. Flow straighteners at the model boundaries provided a uniform initial velocity distribution with relatively low turbulence levels. Portions of the prototype structure with outside dimensions greater than 3 inches, such as pipes, columns, conduit supports, and a stairway, in the immediate vicinity of the sump and below the water surface were modeled to the geometric scale, as shown in Figure 6.

The model was constructed using a combination of wood, steel, and clear acrylic, which allowed observation of flow patterns. One clear acrylic sump is shown in Photograph 4 with the RHR spray suction line. Horizontal suction pipes were modeled for about 16 pipe diameters, had access ports for vortimeter installation, and had five sets of piezometers for pressure gradeline measurement. ASME standard orifice flowmeters were provided to measure flow in each suction line.

The two containment sumps and nearby details are shown in detail in Photographs 5 and 6. These photographs may be compared to the similar perspectives of the prototype shown in Photographs 1 and 2. Clear PMMA plastic was used for sump covers to allow observation of flow patterns between the screens. Narrow slots were provided in the cover plates to allow screen blockages to be changed without model disassembly. The model screens were chosen on the basis of percent open area. The model outer screens were 3/16 inch mesh with 0.063 inch wire diameter and the inner screens were 1/8 inch mesh with 0.041 inch wire diameter. Model screen Reynolds numbers were greater than 100, which resulted in loss coefficients a few percent greater than the predicted values for the prototype screens. The floor grating used in the model was prototype dimensions.

The flow from the RB spray from the above floor was modeled by a tank with an opening simulating the stairway. Flow was supplied by a 4 inch pipe with orifice meter for flow control.

INSTRUMENTATION AND OBSERVATION TECHNIQUES

Flow Measurement

Flowrates were measured by ASME standard orifice meters and coefficients using air-water manometers for differential pressure measurement.

Pressure Gradelines

Each pressure gradeline in the suction line was measured by a pair of piezometers at five locations in each pipe using air-water manometers with the sump water level as reference pressure. The pressure gradeline was extrapolated to the entrance by a linear least squares (linear regression) curve fit of the pressure measurements. The area average velocity was used to calculate the pipe velocity head, which was added to the extrapolated pressure gradeline. The total head within the sump was determined from a pressure measurement and the velocity head at that location. The pipe total head was subtracted from the sump total head to determine the inlet loss. An entrance loss coefficient was calculated by:

$$K = \frac{\Delta H_i}{\frac{V_{mean}^2}{2g}} \qquad (13)$$

where

K = loss coefficient

ΔH_i = inlet head loss, ft

Pipe Swirl

Average swirl in the suction pipes was measured by cross vane vortimeters. Studies at ARL (22) have shown that a vortimeter with vane diameter 75% that of the pipe diameter best approximates the solid body rotation of the flow. The rate of rotation of the vortimeter was determined by counting the number of blades passing a fixed point in one minute.

An average swirl angle was defined as the arctangent of the maximum tangential velocity divided by the axial velocity. The maximum tangential velocity of the vortimeter is the circumferential path travelled by blade tip per unit time, π D N, and the average swirl angle is defined by:

$$\theta = \arctan \left(\frac{\pi D N}{V_{mean}}\right) \qquad (14)$$

where

N = revolutions per second

D = rotameter diameter, ft

V_{mean} = mean axial velocity

Vortex Activity

Vortex activity was recorded by observing vortex strength on a scale from 1 to 6 (see Figure 7). Vortex strength was identified by using dye injection and addition of "trash" consisting of a slightly buoyant ball of paper.

Observation of Flow Patterns

Visual aids, such as dye, were used to observe flow patterns. Photographic documentation was taken whenever appropriate.

TEST PROCEDURE

Tests were conducted at the normal laboratory water temperature. The model was filled to an appropriate level, and all piezometer and manometer lines were purged of air and zero flow differentials checked. The required flowrates were then set and the water level allowed to stabilize. The water level was checked and adjustments made if required and flowrates were rechecked and re-adjusted, if necessary. A 15 minute minimum settling time was allowed prior to initiation of the data recording. Fifteen minutes of vortex observations were recorded and the required physical parameters, such as depth, manometer deflections, and vortimeter readings, were recorded. Entrance losses were determined for the suction lines without vortimeters.

TEST RESULTS

Six floor grating blockages, see Figures 8 through 10, and 8 screen blockages, see Figures 11 through 14, were used in the test program. The approach flow distribution was varied by blocking 50% of the flow straightener area on one side at a time. Various combinations of floor grating blockage, screen blockage, and approach flow distribution were tested. The floor grating was removed to determine whether it had an effect on the vortex activity.

Vortimeters were located in the west containment sump inlet lines and the inlet pipe pressure gradelines were measured in the southwest containment sump lines. Screen losses were measured for all four inlet lines. [redacted]

Vortex Activity

Table 1 summarizes vortex activity for the 76 tests conducted. Maximum activity was a surface dimple, type 2, indicating some swirl at the surface. Dye injection indicated the dimple to be a surface phenomenon and no coherent core was detectable, even at the surface. In only one case of 33 using Froude scale velocity was a surface dimple noted. For prototype velocity, this increased to 23 cases of a total of 43. In all cases, the surface dimple was unstable and was carried across the sump by the general circulation patterns and quickly dissipated. Dimples over the west sump were caused by vortices shed from the support columns, which translated across the sump. Over the southwest sump, the vortices were generated by the columns and piping in the area. Due to the approach path and local geometry, a general clockwise circulation developed over the southwest containment sump. This circulation became somewhat more pronounced when the south flow straightener was 50% blocked.

Removal of the floor grating did not increase vortex activity. Combined floor grating and screen blockages caused the greater vortex activity. Approach flow distribution had little effect on vortex activity.

TABLE 1

Vortex Activity

Test Number		Floor	Screen		Velocity Scale			
					Froude		Prototype	
F	P	Grating	Blockage	FF	West	Southwest	West	Southwest
1	6			0	1	1	1	1
2				1	1	1		
3				1	1	1		
4				2	1	1		
5				2	1	1		
	7	1		0			1	1
	8	2		0			1	1
	9	3		0			1	2
	10	4		0			1	2
	11	5		0			1	1
	12	6		0			1	1
	13		1	0			1	2
	14		2	0			1	1
	15		3	0			1	2
	16		4	0			1	1
	17		5	0			1	1
52	18		6	0	1	1	1	1
	19		7	0			1	
	20		8	0			1	1
38	21	1	8	0	1	1	1	1
37	22	1	8	1	1	1	1	2
38	23	1	8	2	1	1	1	1
33	24	4	8	0	1	1	2	2
34	25	4	8	1	1	1	2	2
35	26	4	8	2	1	1	2	2
32	27	6	8	0	1	1	1	1
31	28	6	8	1	1	1	1	2
30	29	6	8	2	1	1	1	1
56	62	1	2	0	1	1	1	1
57	63	4	2	0	1	1	2	2
58	64	6	2	0	1	1	1	1
59	65	1	4	0	1	1	2	1
40		1	4	2	1	1		
41		1	4	1	1	2		
42	66	4	4	0	1	1	2	2
43		4	4	2	1	1		
44		4	4	1	1	1		
45	67	6	4	0	1	1	1	2
46		6	4	1	1	1		
47		6	4	2	1	1		
53	68	1	6	0	1	1	1	2

TABLE 1
(continued)

Test Number		Floor	Screen		Velocity Scale			
					Froude		Prototype	
F	P	Grating	Blockage	FF	West	Southwest	West	Southwest
	69	2	6	0			1	2
	70	3	6	0			2	2
54	71	4	6	0	1	1	2	2
	72	5	6	0			1	2
55	73	6	6	0	1	1	2	1
48	59	None	4	0	1	1	2	
49	61	None	4	1	1	1	1	1
50	60	None	4	2	1	1	1	1
51	77	None	6	0	1	1	1	2
	78	None	6	0			1	2
	79	None	2	0			1	1

See Figures 8 through 14 for floor grating and screen blockage configurations.

For Approach Flow Distribution, (FF) indicates no flow straightener blockage, 1 indicates west blocked 50%, and 2 indicates south blocked 50%.

Swirl Angle Measurements

Rotameter rotation rates were used to calculate swirl angles by Equation (14). Rotameters were located in the RHR and RBS lines in the west containment sump for all tests. Rotameter rotation rates were unsteady for several tests with reversing direction during the one minute observation period. In these cases, the greater rotation rate was used to calculate swirl angle and, therefore, in some tests opposite rotation directions appear for Froude and prototype velocity scale tests.

Appendix B lists the calculated swirl angles, blockage configurations, and approach flow distributions for all tests conducted. Approach flow distribution had little effect on swirl angle when floor grating and screen blockage were combined. Floor grating blockage had little effect when screen blockage were in place, with the exception of the horizontal screen blockage which imparted no swirl. Table 3 summarizes the swirl angles averaged for each screen blockage, since screen blockage was the dominant factor in most cases.

TABLE 3

Average Swirl Angles, Degrees

Screen Blockage*	RHR Inlets	RB Spray Inlet
None	3.2	2.4
None, all floor grating blockages	1.8	4.3
All screen only	4.7	3.6
2	4.8	3.5
4	4.8	5.5
6	1.9	1.8
8	2.8	4.1
4 without floor grating	5.7	5.0

*See Figures 8 through 14 for screen blockage configurations

The swirl angles for the RHR and RBS inlets were 3.2 and 2.4 degrees, respectively, for clean screens. Screen blockage configuration 4 created the greatest average swirl with values of 4.8 and 5.5 degrees for the RHR and RBS inlets, respectively. With the floor grating removed, the swirl angles were similar, 5.7 and 5.0 degrees.

The maximum swirl angle measured was 9.5 degrees for screen blockage configuration 3. Average swirl angles for all tests were 3.6 degrees for the RHR inlet and 3.9 degrees for the RBS inlet.

Since about 48 diameters of straight pipe exists prior to any fittings in the inlet lines, the swirl angle will decay considerably. Using a conservative estimate for the swirl decay parameter, $\beta = 0.02$, from available literature (27, 28), the swirl remaining at the end of the straight pipe will be about 40 percent of the initial swirl. This results in a maximum swirl angle of 3.8 degrees and average swirl angles of less than 2 degrees. Swirl angles of similar magnitudes may result from single bends (24) and swirl angles resulting from combined bends could be about three times greater (25, 26). Therefore, the measured swirl angles are not considered excessive.

Screen Head Loss

The head losses due to the floor grating and two sets of screens were measured for all four pump inlets for all tests. The velocity head of the approach flow was neglected such that the measured water level outside the screens was assumed to be the initial total head. Static head was measured in each sump with two piezometers at elevation 404 ft. The velocity head in the sump, calculated using the area average velocity, was added to the static head to determine the total head. Screen loss was determined by subtracting the sump total head from the measured water level. The measured head loss was corrected to the runout flowrate for each pump and converted to prototype dimensions.

As a check, the RHR screen losses were calculated (8). For clean screens, the calculated loss was less than 0.01 ft and with the screens 50% blocked, the calculated loss was less than 0.03 ft. These values are based on approach flow normal to the screen with a relatively uniform approach velocity distribution. Actual losses will be considerably greater due to the complicated approach flow path which has several changes in direction due to the orientation of the floor grating and the vertical offset of the screens. With blockage, horizontal screen offsets could also be included. The magnitudes of the screen losses are small in relation to experimental uncertainty and, therefore, averages will be used to illustrate losses.

Appendix A lists the measured losses for all tests for the four pump inlets. Table 2 summarizes the average loss measurements. Floor grating blockage and non-uniform approach flow distribution did not cause losses to vary greatly. Screen blockage could cause losses to vary due to the flow path variations. Therefore, losses for a given screen blockage are averaged over floor grating blockage and approach flow distribution configurations.

TABLE 2

Screen Loss Summary

	Loss - Feet	
Screen Blockage*	RHR	RB Spray
None	0.06	0.05
None, all floor grating blockages	0.06	0.04
2	0.10	0.06
4	0.09	0.05
6	0.08	0.05
8	0.10	0.06
4 without floor grating	0.09	0.05

*See Figures 11 through 14 for screen blockage configurations.

Clean screen losses averaged 0.06 ft for the RHR inlet and 0.05 ft for the RB spray inlet. Tests with floor grating blockages resulted in losses of 0.06 ft and 0.04 ft for the RHR inlet and the RB spray inlet, showing little change. The four screen blockage configurations with sufficient data to average resulted in an increased loss of about 0.03 ft for the RHR inlet and about 0.1 ft for the RBS inlet. For the RHR inlet, the increase is about what was calculated for the blocked screen losses. The losses due to the flow path are significantly higher than the screen losses. In the case of the RBS inlet, the losses should be about 45 percent of the RHR inlet losses, due to the decreased flow. The measured losses were somewhat high in comparison to the RHR inlet loss, but the increase due to screen blockage was near what would be calculated.

Inlet Losses

Inlet losses were measured and an inlet loss coefficient was calculated by Equation (13). The inlet loss coefficient was essentially equal for the RHR and RBS inlets and had a value of 0.27. This compares well to published data (23) and data from previous studies (29). The head losses were 0.37 ft and 0.30 ft for the RHR inlet and the RBS inlet, respectively.

Flow from Mezzanine Floor Level

Tests were conducted with flow from the mezzanine floor stairwell opening to determine whether any adverse conditions, such as bubble formation and subsequent air entrainment, might exist. A series of flowrates were used with the maximum flowrate of 1300 gpm corresponding to a depth of about six inches on the mezzanine floor. Since the mezzanine floor has a six inch curb around all openings, significantly greater depth would be impossible. The flow pattern from the stairwell is shown in Photograph 7 for the maximum flowrate. The first flight of stairs was modeled and they deflected the majority of the flow vertically downward. The stairwell entrance is between the fan duct wall and the bioshield wall, therefore, the majority of the flow fell into the fan duct. The flow that was able to travel horizontally enough to impact in the front of the fan duct wall was

distributed over a large area. The remainder of the stairway, not modeled in these tests, would further dissipate the energy of the falling water and further spread the impact area. No air bubbles penetrated the water surface sufficiently to be detectable in the sump area. As the flowrate and depth on the mezzanine floor decreased to 990 gpm, the initial horizontal velocity decreased and less flow impacted outside the fan duct. At the 4 inch depth corresponding to a flowrate of 680 gpm, only a small amount of flow impacted outside the fan duct, as shown in Figure 9. Flow from the mezzanine floor level did not cause any adverse effects.

SUMMARY

A 1:2.9 scale model of the containment building sump for the Virgil C. Summer Nuclear Station was constructed and tested. In the recirculation mode, residual heat removal and reactor building spray pumps withdraw water from two containment sumps after a postulated loss of coolant accident. A horizontal floor grating, 1/2 and 1/4 inch mesh vertical screens, surround each pump sump to assure no debris is entrained into the pumping systems. The debris could block both the floor grating and screens, thereby producing adverse flow patterns in the sump. A wide range of possible approach flow distributions, floor grating blockages, and screen blockages, and combinations thereof were tested to simulate possible undesirable flow patterns which could result in poor pump performance during the recirculation mode. The model was operated with both Froude scale velocity and prototype velocity. Vortex activity was observed and recorded. Head losses due to the floor grating, screens, and pump inlet and the flow rotation in the suction pipe were also measured.

A surface dimple was the greatest vortex activity observed. For Froude scale velocity, only one test in 33 had a surface dimple. Increasing the velocity to prototype velocity increased vortex activity such that in about one-half of the 43 cases a surface dimple formed. The surface dimples noted were produced from vortices shed from obstructions in the flow, such as support columns and, therefore, traveled with the general flow patterns. No coherent dye core formed in conjunction with the surface dimple. Tests without the floor grating showed no increase in vortex activity.

Average swirl angle in the suction pipes was less than 4 degrees and maximum value measured was 9.5 degrees. Screen losses varied from about 0.05 ft for a clean screen to 0.19 ft for the worst case of 50 percent screen blockage. The pipe inlet head loss averaged about 0.3 times the inlet pipe velocity head.

REFERENCES

1. Daggett, L.L., and Keulegan, G.H., "Similitude Conditions in Free Surface Vortex Formations," Journal of Hydraulics Division, ASCE, Vol. 100, pp. 1565-1581, November 1974.

2. Daily, J.W., and Harleman, D.R.F., Fluid Dynamics, Addison-Wesley Publishing Company, 1965.

3. Rouse, H., Handbook of Hydraulics, John Wiley & Sons, 1950.

4. Anwar, H.O., Weller, J.A., and Amphlett, M.B., "Similarity of Free-Vortex at Horizontal Intake," Journal of Hydraulic Research, IAHR 16, No. 2, 1978.

5. Hattersley, R.T., "Hydraulic Design of Pump Intakes," Journal of the Hydraulics Division, ASCE, pp. 233-249, March 1965.

6. Reddy, Y.R., and Pickford, J., "Vortex Suppression in Stilling Pond Overflow," Journal of Hydraulics Division, ASCE, pp. 1685-1697, November 1974.

7. Durgin, W.W., Neale, L.C., and Churchill, R.L., "Hydrodynamics of Vortex Suppression in the Reactor Building Sump Decay Heat Removal System," ARL Report No. 46-77/M202FF, February 1977.

8. Baines, W.D., and Peterson, E.G., "An Investigation of Flow Through Screens," Trans. ASME, pp. 467-477, July 1951.

9. Papworth, M., "The Effect of Screens on Flow Characteristics," British Hydromechanics Research Association, Report TN1198, November 1972.

10. Weighardt, K.E.G., "On the Resistance of Screens," The Aeronautical Quarterly, Vol. IV, February 1953.

11. Tennessee Valley Authority, "Flow Through Screens," Report No. 87-8, May 1976.

12. Padmanabhan, M., "Hydraulic Model Studies of the Reactor Containment Building Sump, North Anna Nuclear Power Station - Unit 1," ARL Report No. 123-77/M250CF, July 1977.

13. Govier, G.W., and Aziz, K., "The Flow of Complex Mixtures in Pipes," Van Nostrand Reinhold, 1972.

14. Chainshvili, A.G., "Air Entrainment and Vertical Downward Motion of Aerated Flows," IAHR, 8th Congress, Montreal, Canada.

15. Muakami, M., Suehiro, H., Ieiji, T., and Kajita, J., "Flow Entrained Air in Centrifugal Pumps," 13th Congress, IAHR, Japan, August 31 - September 5, 1969.

16. Final Safety Analysis Report, J.M. Farley Nuclear Plant, Appendix 60, Nuclear Regulatory Commission, 1977.

17. Durgin, W.W., and Hecker, G.E., "The Modeling of Vortices at Intake Structures," Joint Symposium of Design and Operation of Fluid Machinery, Colorado State University, June 1978.

18. Padmanabhan, M., "Hydraulic Model Investigation of Vortexing and Swirl Within a Reactor Containment Recirculation Sump," Donald C. Cook Nuclear Power Station, ARL Report No. 108-78/M178FF.

19. Padmanabhan, M., "Assessment of Flow Characteristics Within a Reactor Containment Recirculation Sump Using a Scale Model," McGuire Nuclear Power Station, ARL Report No. 29-78/M208JF.

20. Padmanabhan, M., "Selection and Scaling of Horizontal Gratings for Vortex Suppression," ARL Report No. 68-78, July 1978.

21. Padmanabhan, M., and Vigander, S., "Pressure Drop Due to Flow Through Fine Mesh Screens," Journal of the Hydraulics Division, ASCE, HY8, August 1978.

22. Durgin, W.W., and Lee, H.L., "The Performance of Cross-Vane Swirl Meters," ASME Winter Annual Meeting, 1980.

23. Miller, D.S., Internal Flow Systems, BHRA Fluid Engineering, 1978.

24. Unpublished ARL Experimental Results.

25. Padmanabhan, M., "Investigation of Flow Distribution and Swirl Due to a Combined Pipe Bend," McGuire Nuclear Power Station, ARL Report No. 12-79/M208MF, December 1978.

26. Nystrom, J.B., "The Effects of Combined Bends on the Velocity Distribution and Swirl at the Inlet to a Pump," ARL Report No. 122-80/M105AF, August 1980.

27. Baker, D.W., and Sayre, C.L., "Decay of Swirling Turbulent Flow of Incompressible Fluids in Long Pipes," Flow, Its Measurement and Control in Science and Industry, 1974.

28. Janik, C.R., and Padmanabhan, M., "The Effect of Swirling Flow on Pipe Friction Losses," ARL Report No. 26-81/M296KF, February 1981.

29. Padmanabhan, M., "Investigation of Vortexing and Swirl Within a Containment Recirculation Sump Using a Hydraulic Model," ARL Report No. 25-81/M296HF, February 1981.

FIGURES

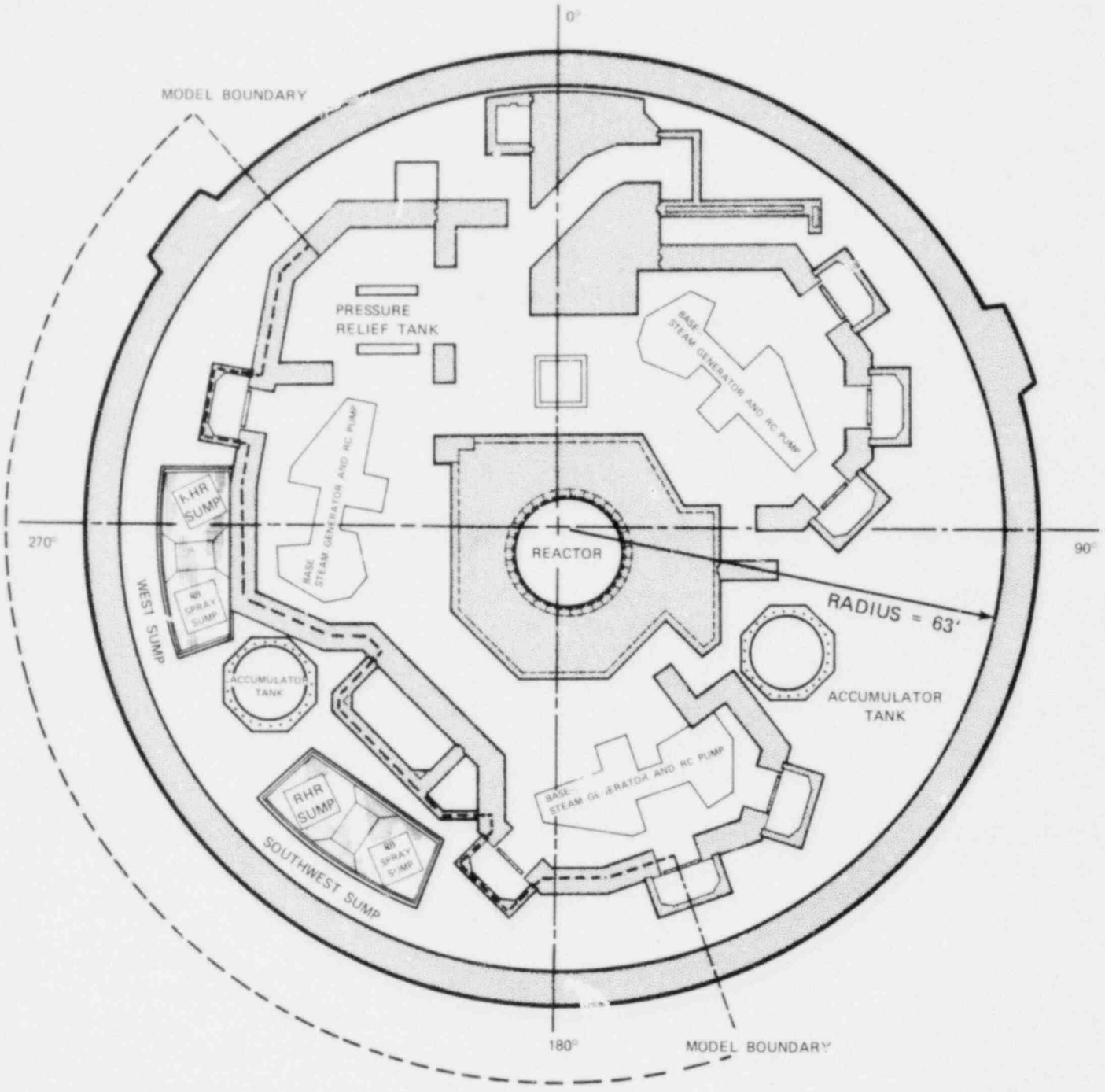

FIGURE 1 REACTOR BUILDING LAYOUT AT EL 412 FEET

ARL

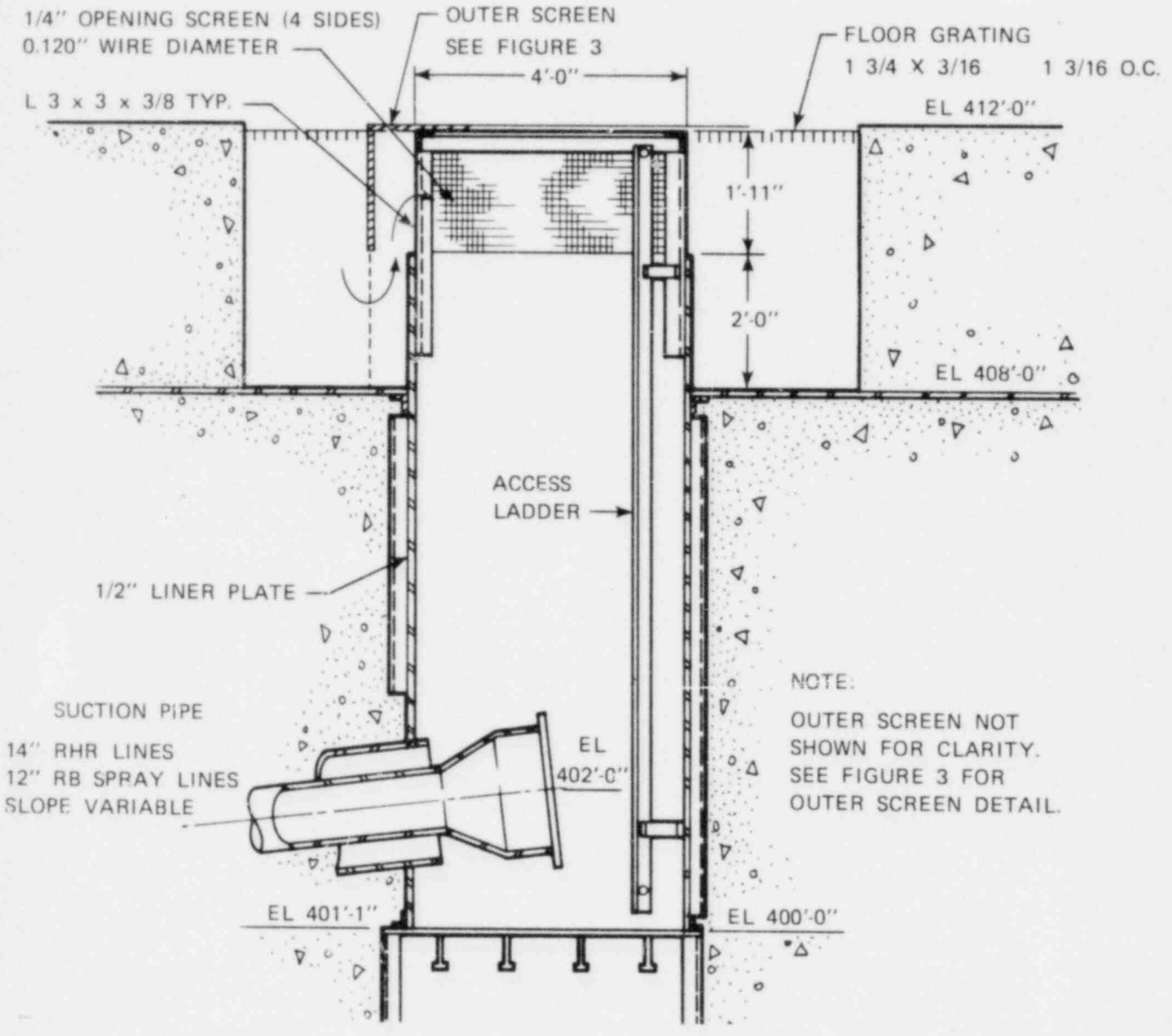

FIGURE 2 SECTION OF SUCTION PIPE SUMPS AND INNER SCREENS

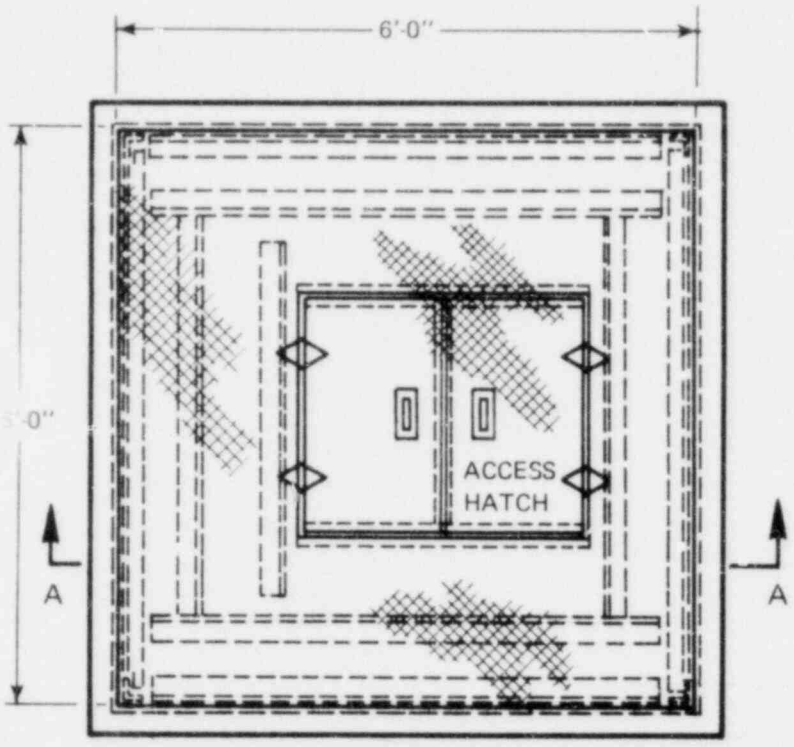

PLAN VIEW

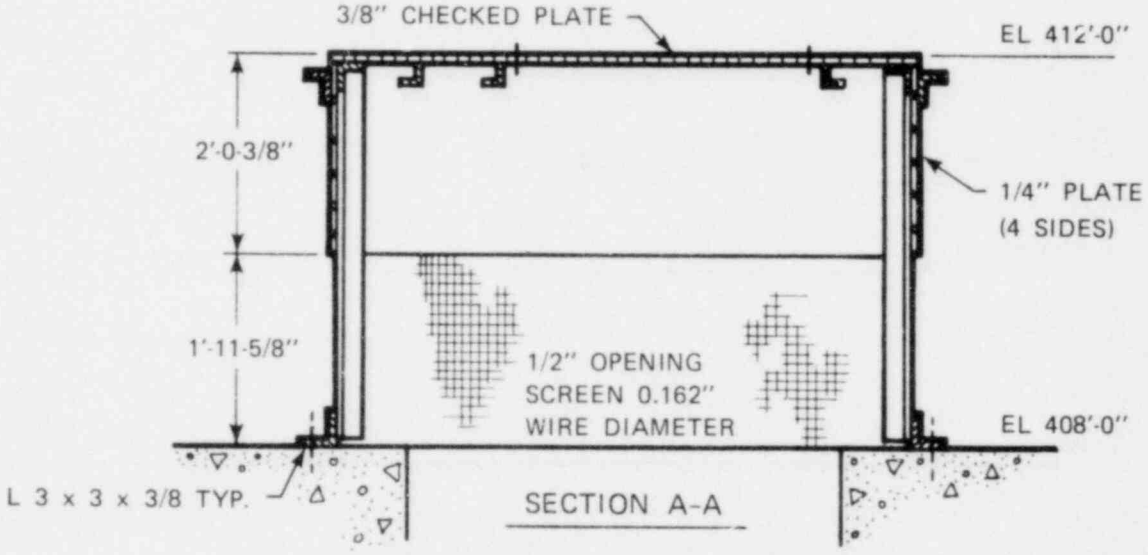

SECTION A-A

FIGURE 3 OUTER SCREEN DETAILS

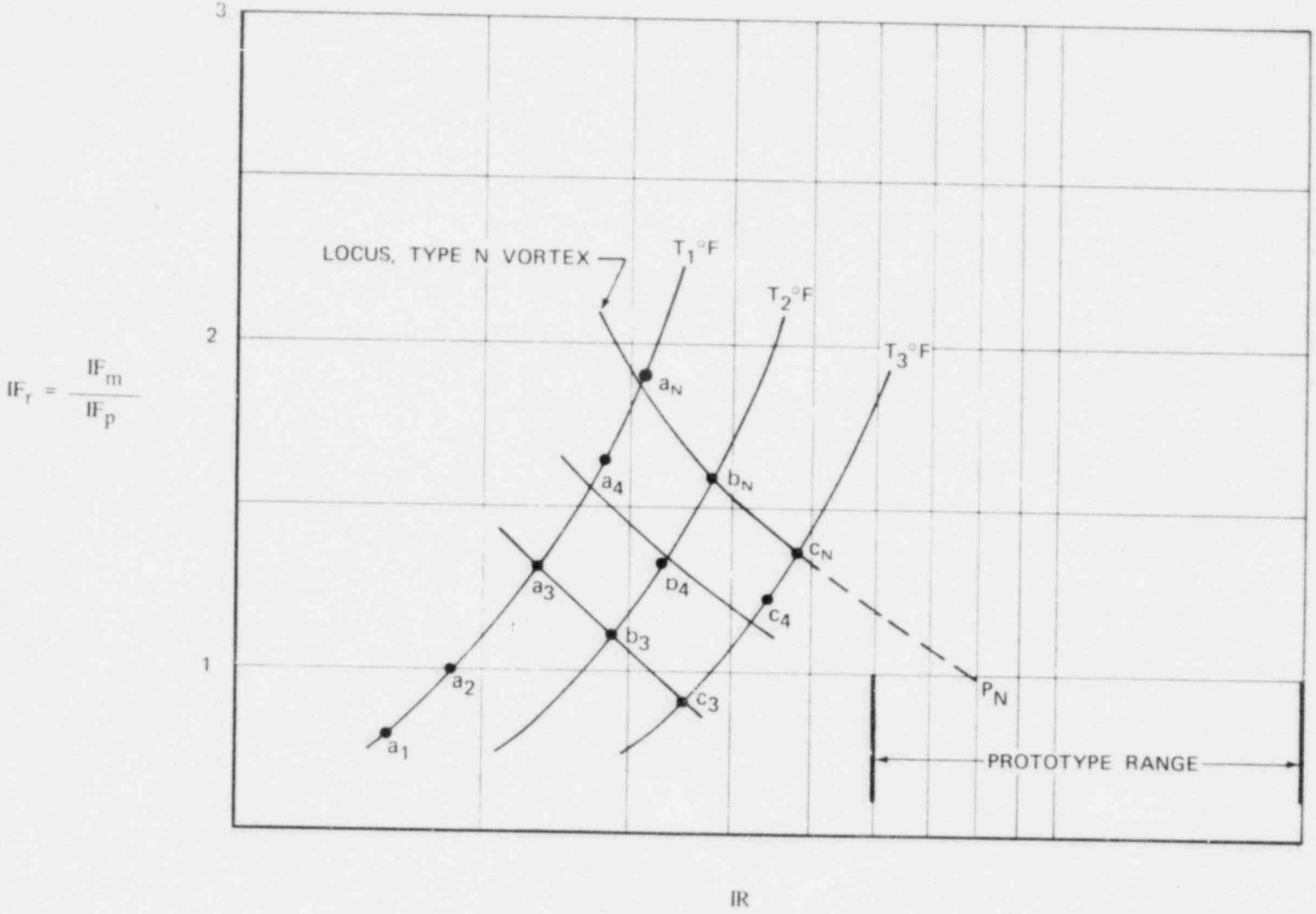

FIGURE 4 ARL VORTEX ACTIVITY EXTRAPOLATION TECHNIQUE

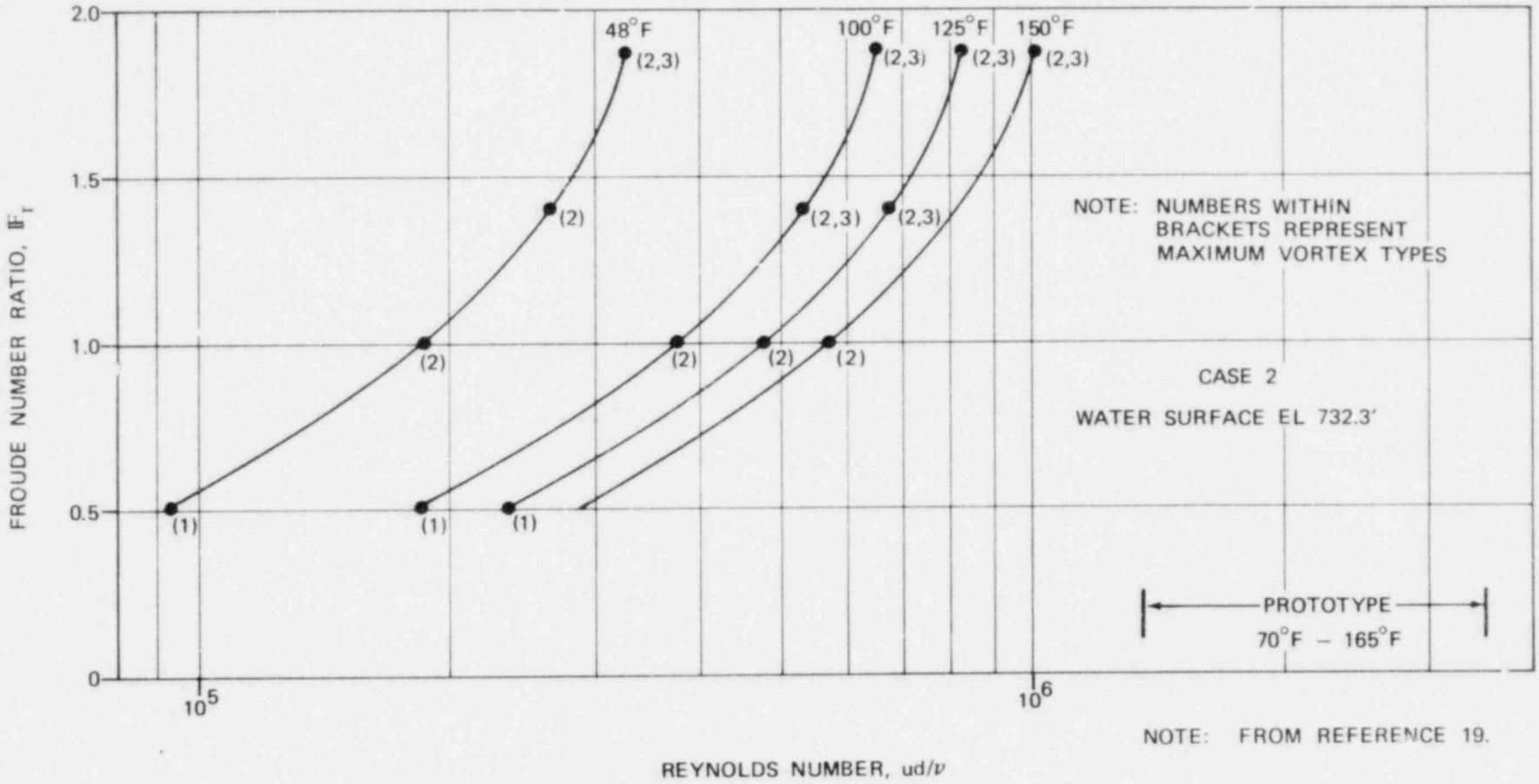

NOTE: FROM REFERENCE 19.

FIGURE 5 TYPICAL MODEL RESULTS FOR ARL VORTEX ACTIVITY EXTRAPOLATION TECHNIQUE

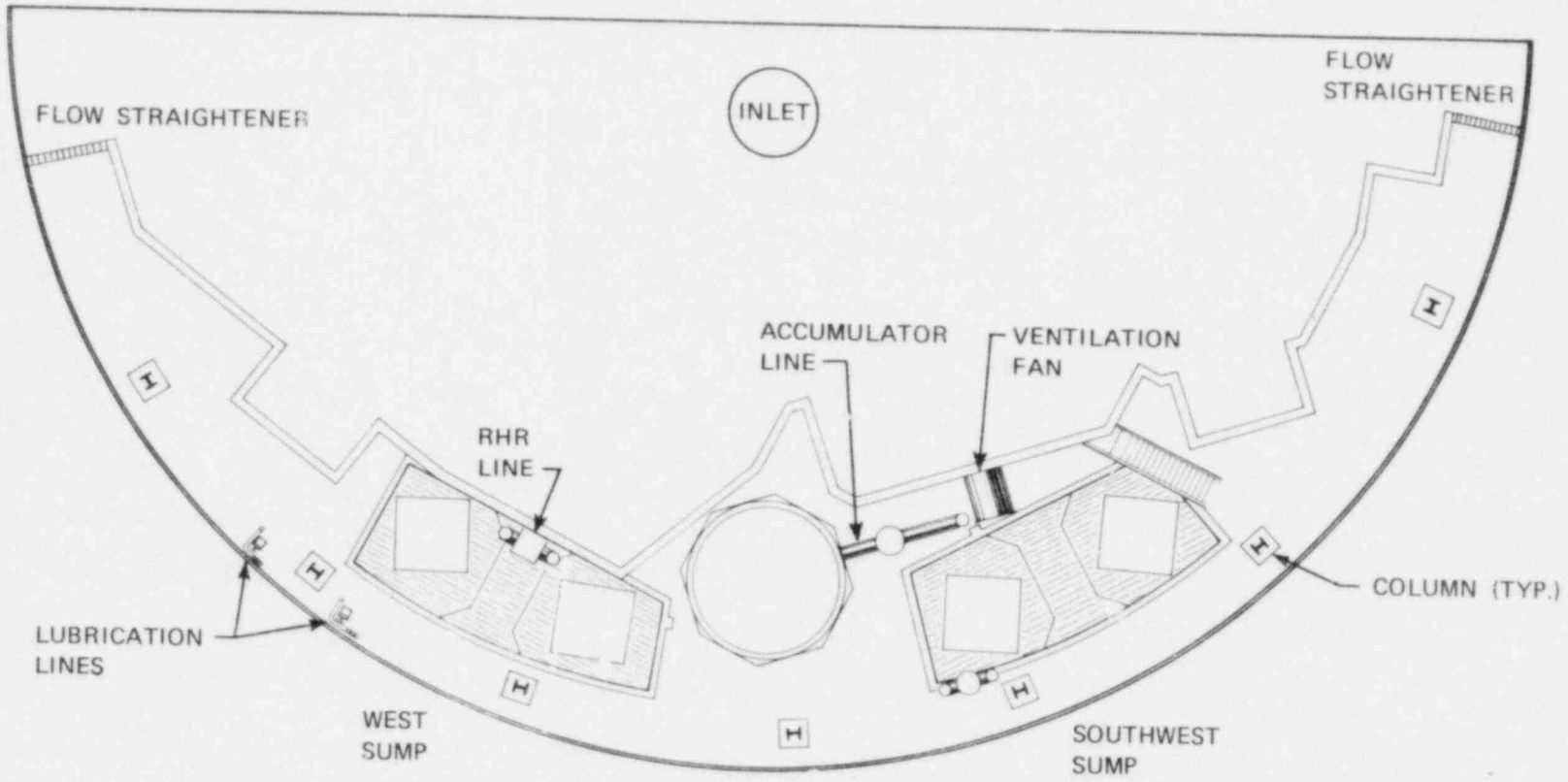

FIGURE 6 PLAN VIEW MODEL WITH DETAILS

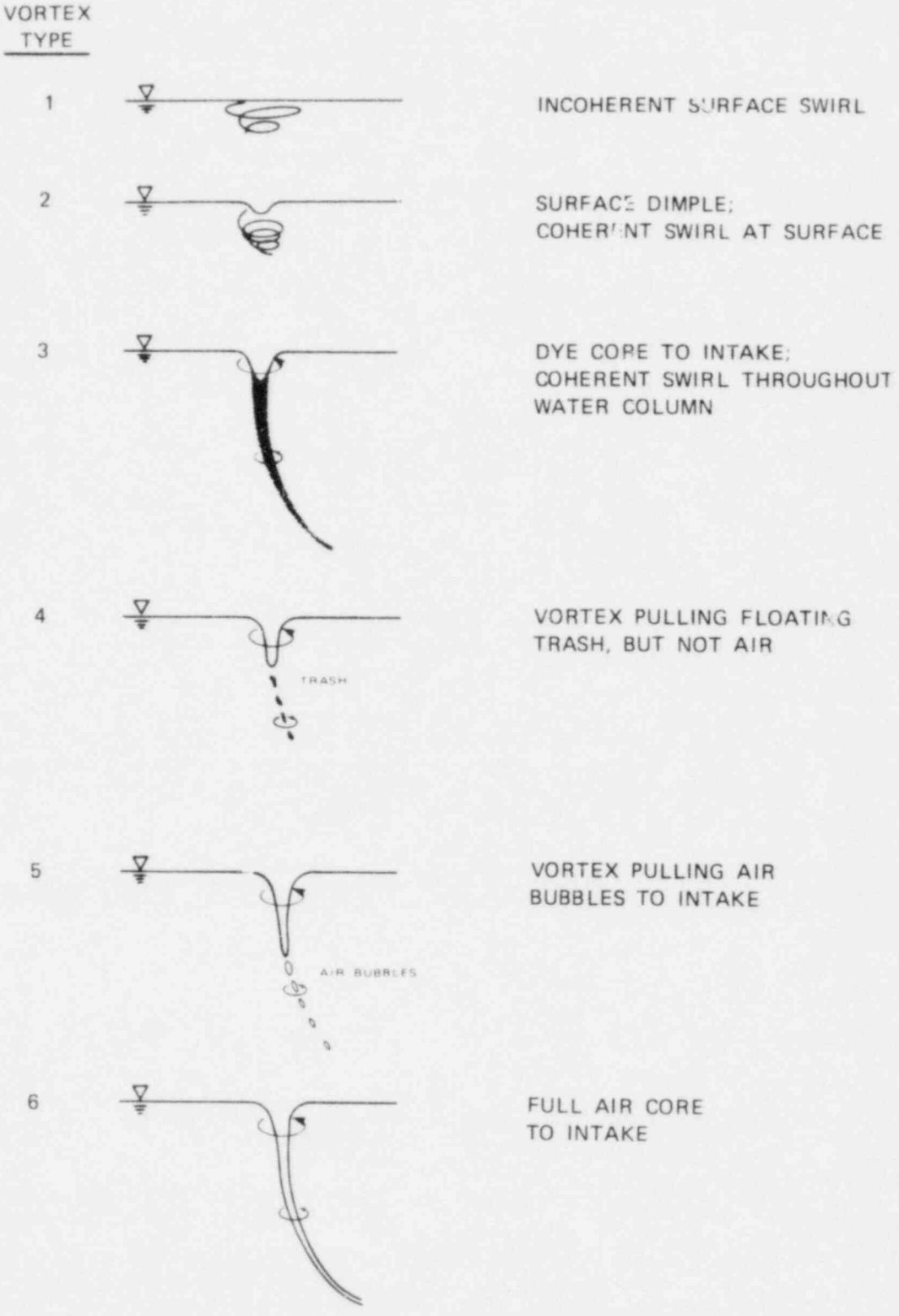

FIGURE 7 CLASSIFICATION OF FREE SURFACE VORTICES

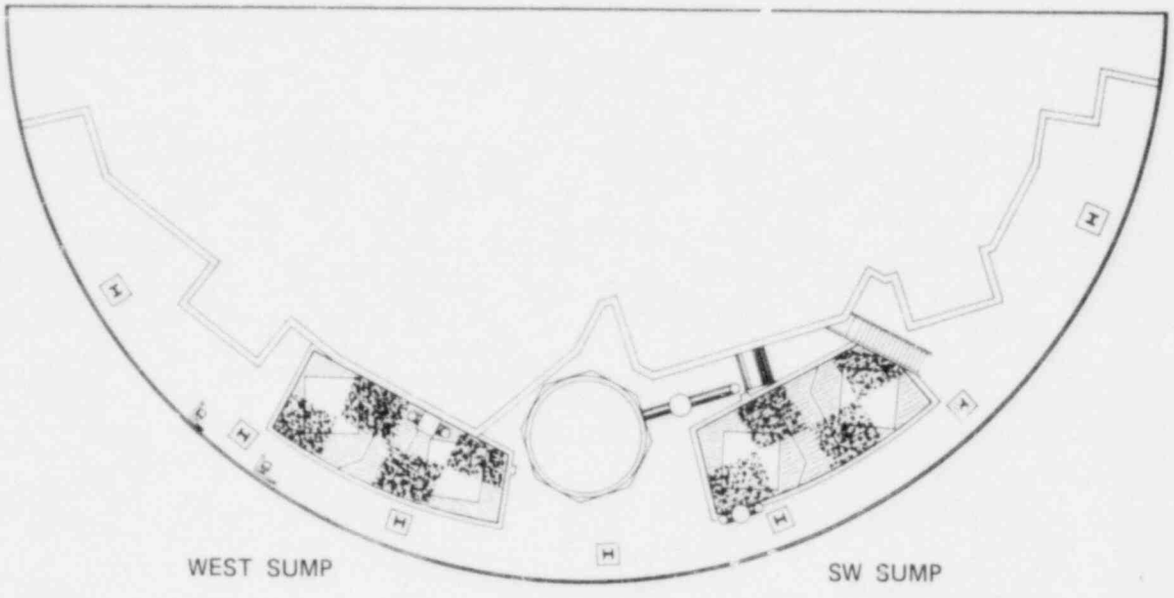

FLOOR GRATING BLOCKAGE 1

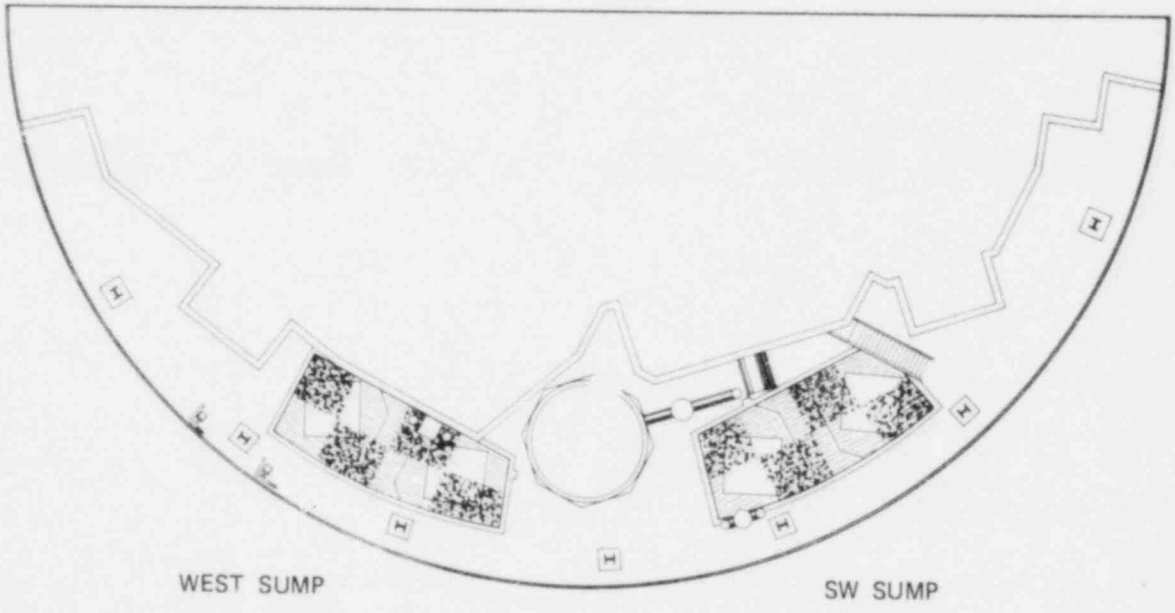

FLOOR GRATING BLOCKAGE 2

FIGURE 8 FLOOR GRATING BLOCKAGE SCHEMES

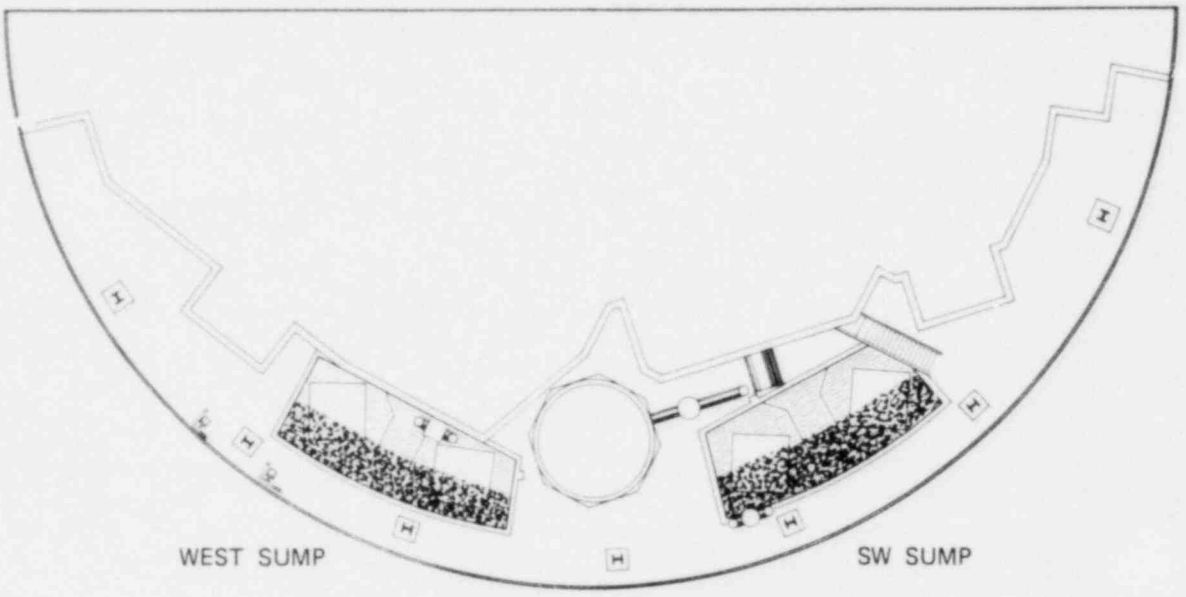

FLOOR GRATING BLOCKAGE 3

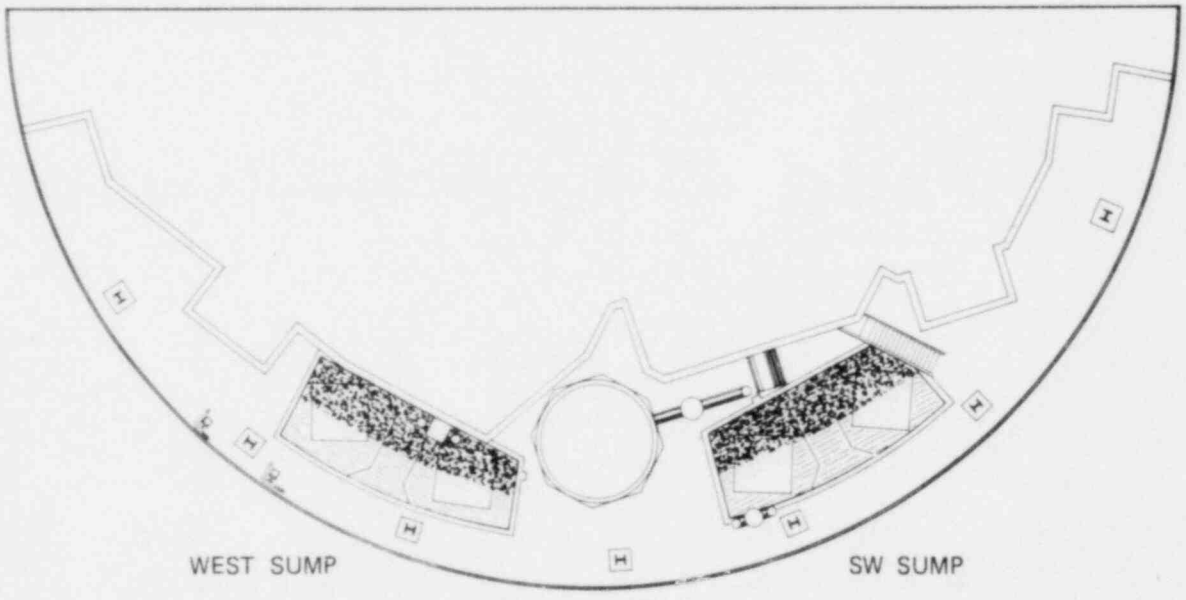

FLOOR GRATING BLOCKAGE 4

FIGURE 9 FLOOR GRATING BLOCKAGE SCHEMES

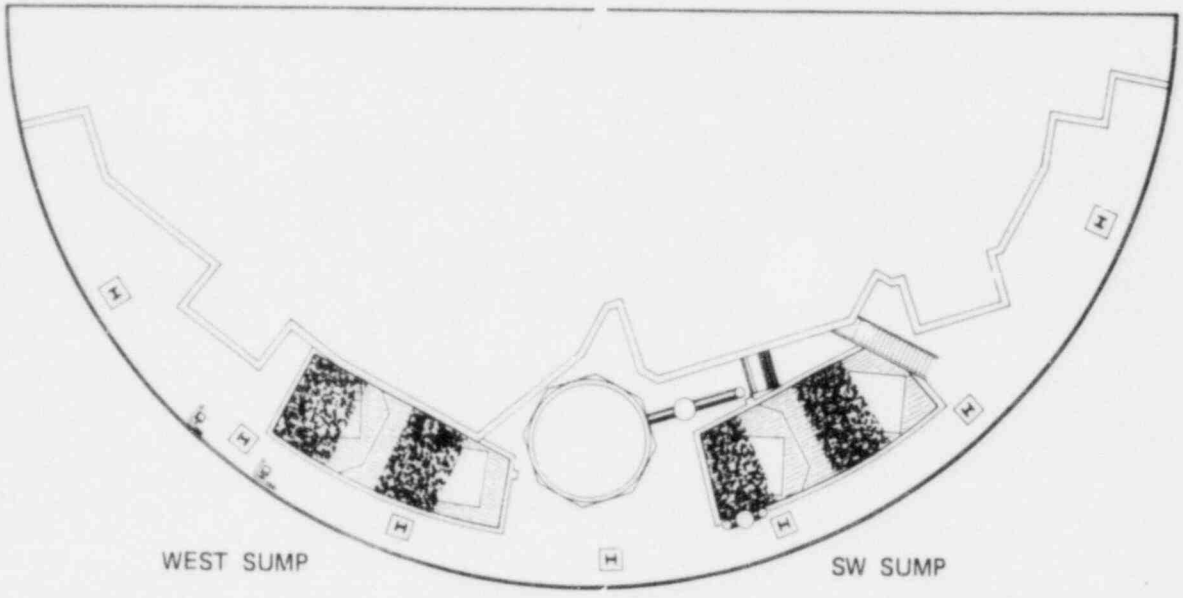

FLOOR GRATING BLOCKAGE 5

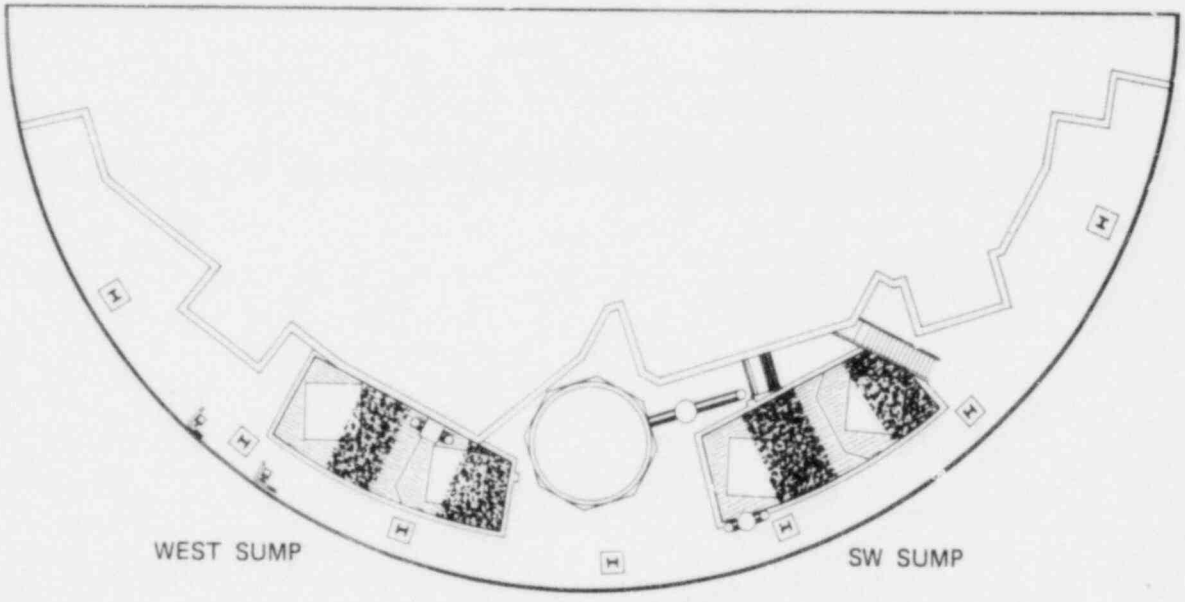

FLOOR GRATING BLOCKAGE 6

FIGURE 10 FLOOR GRATING BLOCKAGE SCHEMES

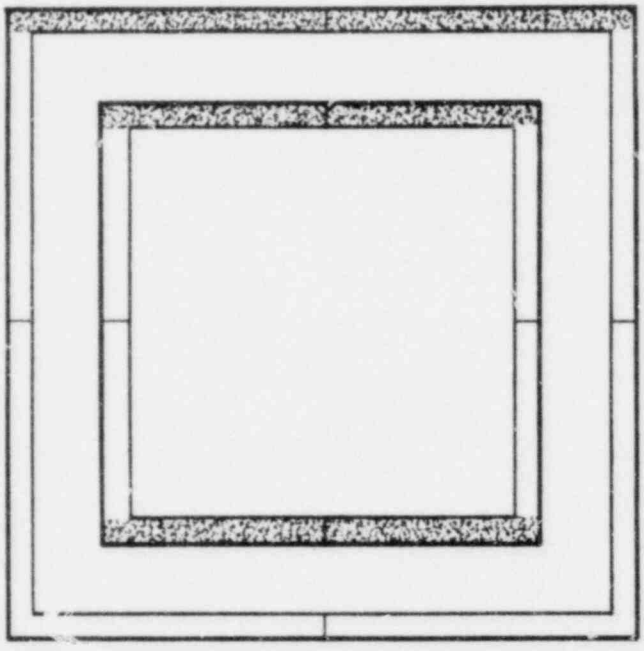

SCREEN BLOCKAGE 1

NOTE: COMPLETELY BLOCKED VERTICALLY
SCREEN ORIENTATION AS IN FIGURE

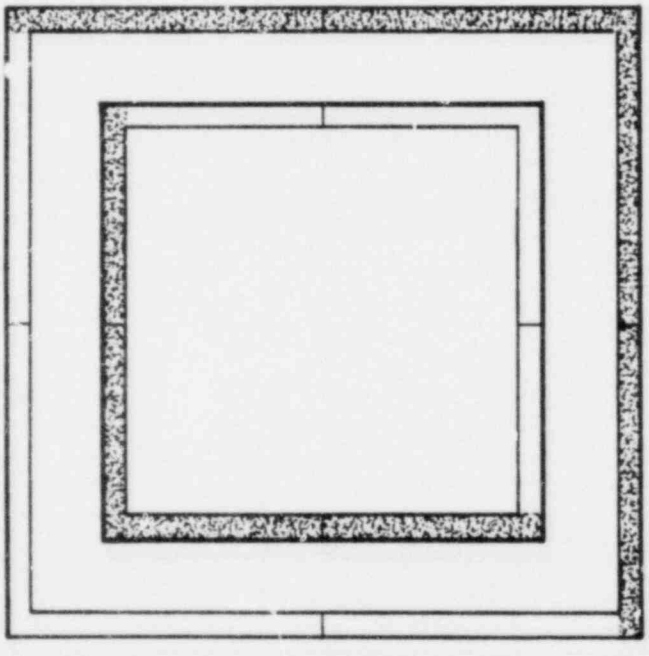

SCREEN BLOCKAGE 2

FIGURE 11 INNER AND OUTER SCREEN BLOCKAGE SCHEMES

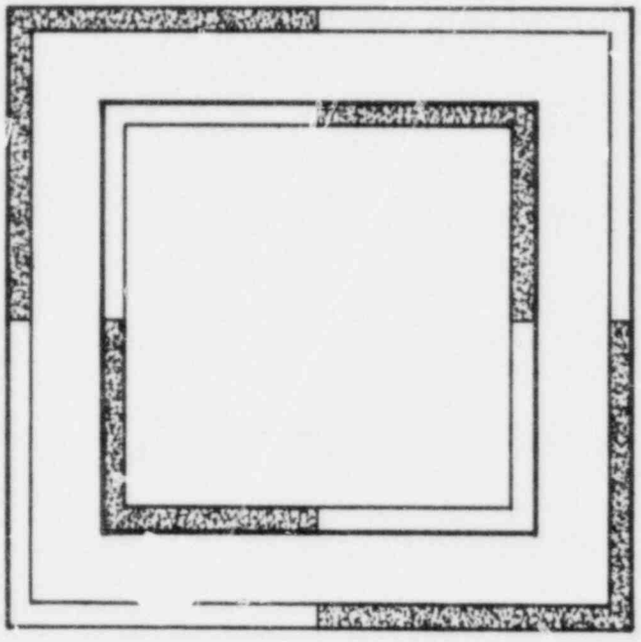

BLOCKAGE 4

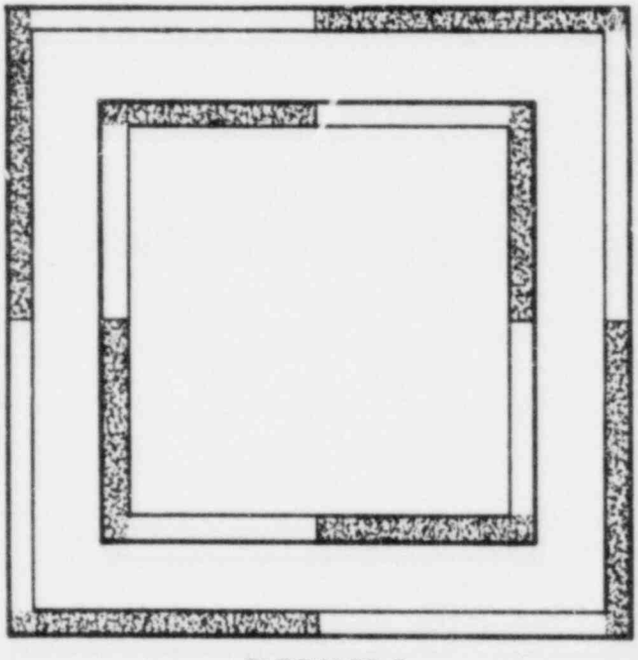

BLOCKAGE 3

FIGURE 12 INNER AND OUTER SCREEN BLOCKAGE SCHEMES

ARL

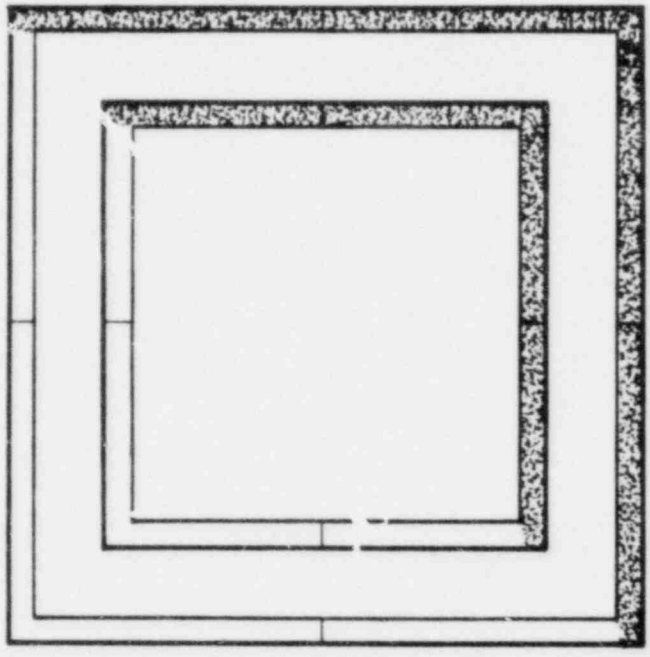

BLOCKAGE 5

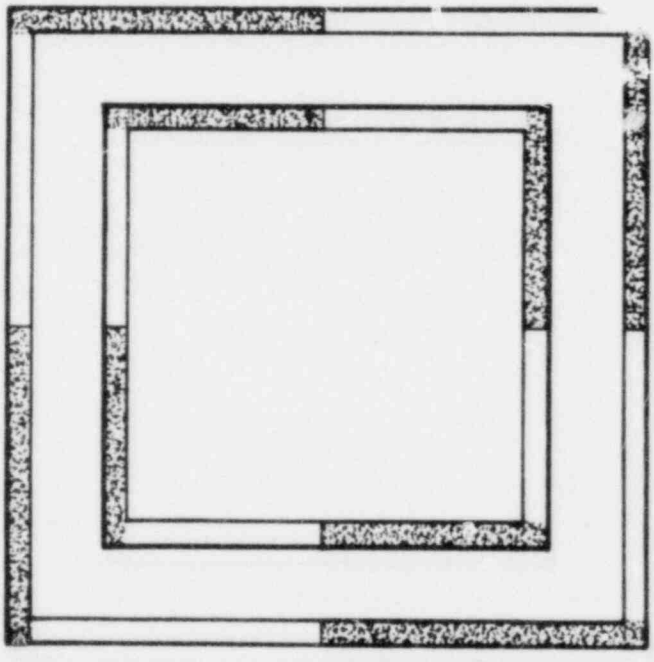

BLOCKAGE 6

FIGURE 13 INNER AND OUTER SCREEN BLOCKAGE SCHEMES

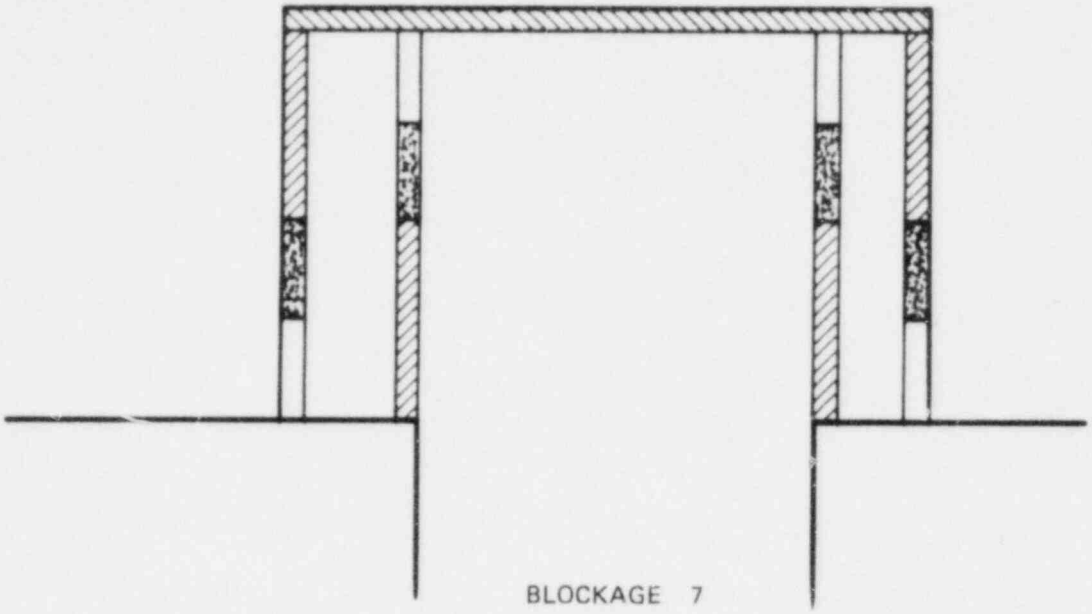

BLOCKAGE 7

NOTE: COMPLETELY BLOCKED HORIZONTALLY.

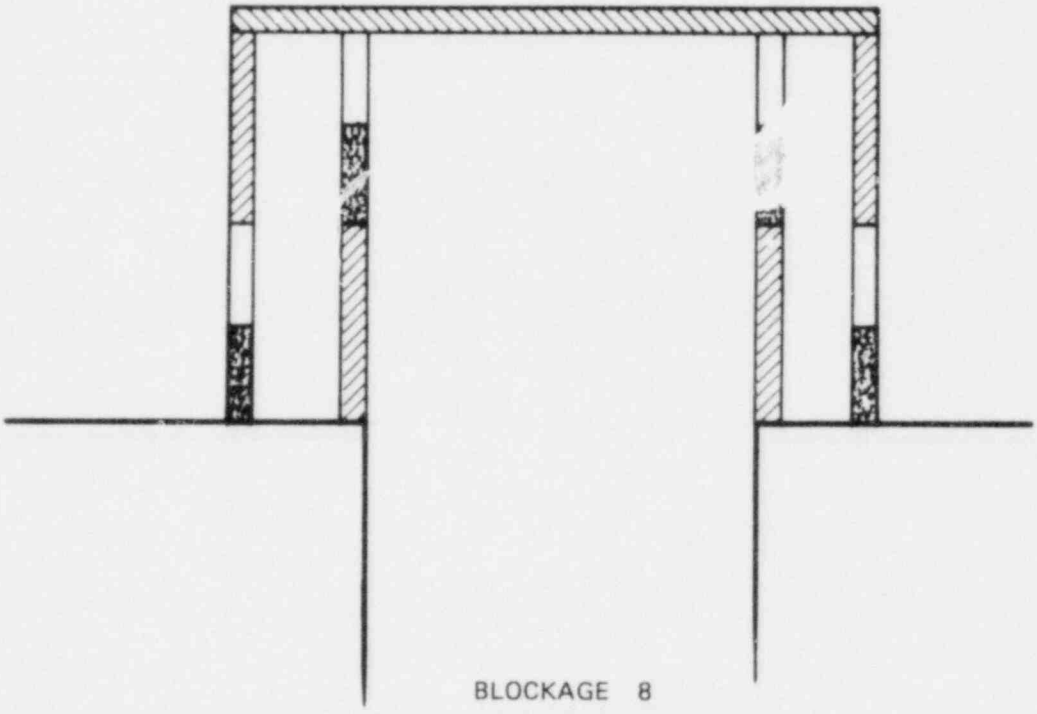

BLOCKAGE 8

FIGURE 14 INNER AND OUTER SCREEN BLOCKAGE SCHEMES

PHOTOGRAPHS

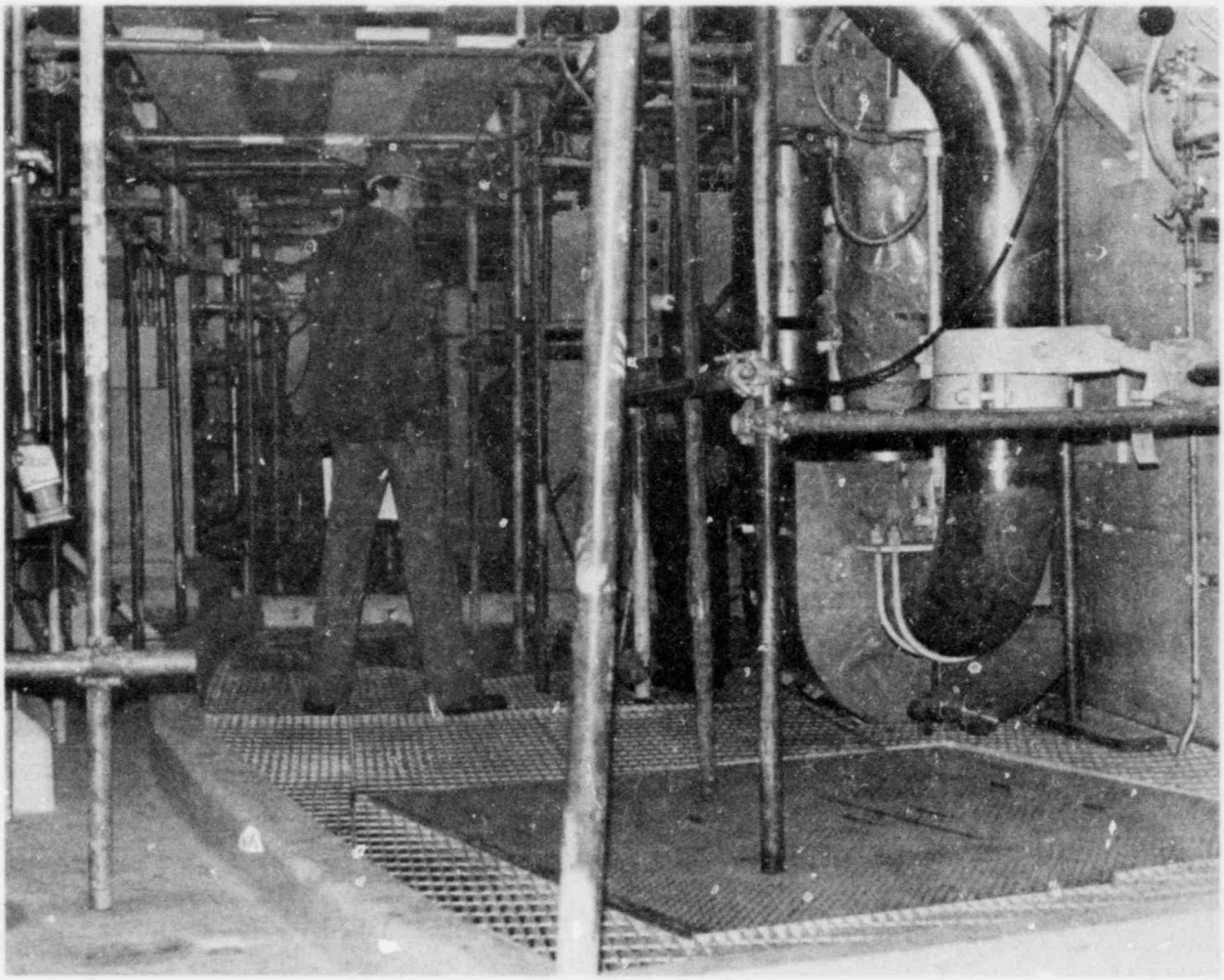

Photograph 1 West Sump – Prototype

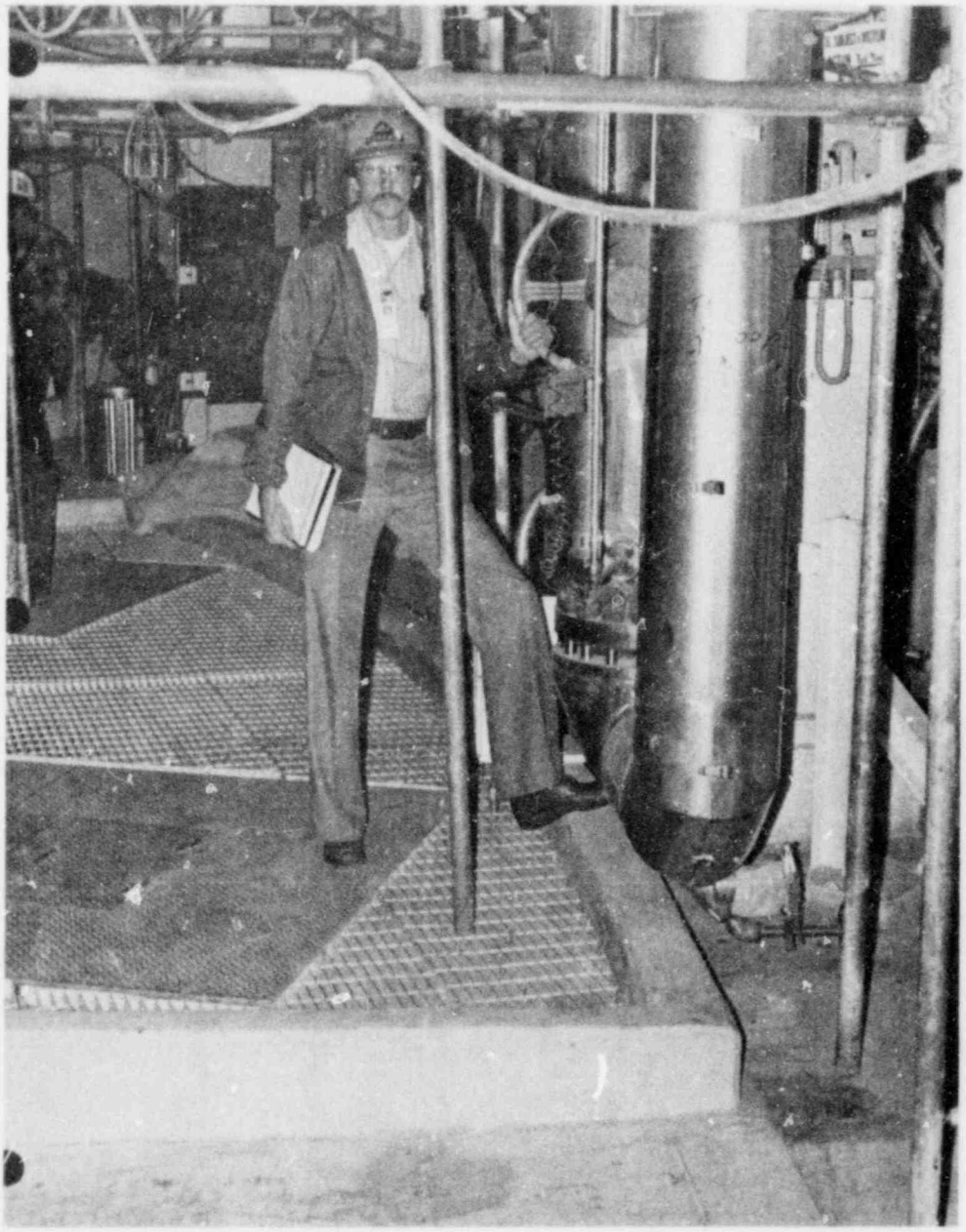

Photograph 2 Southwest Sump – Prototype

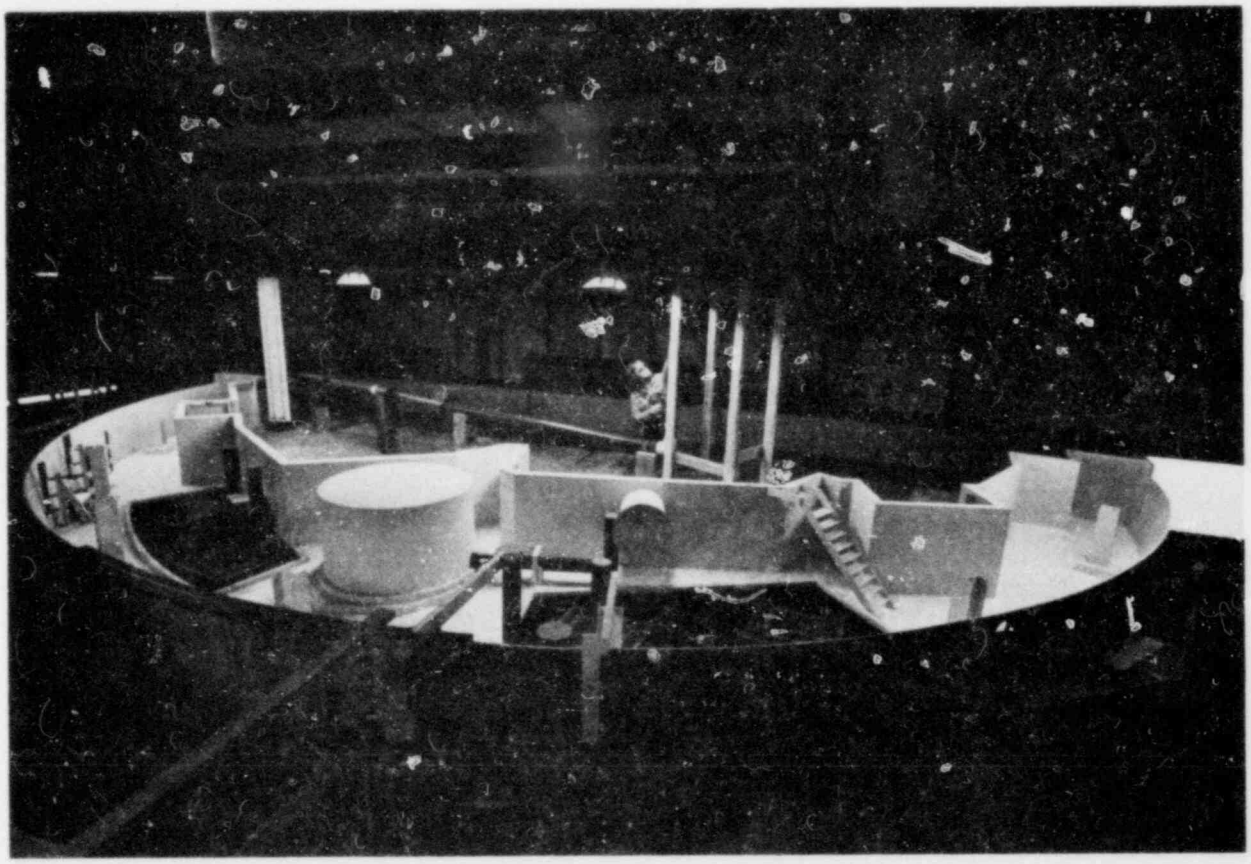

Photograph 3 Overall View of Model

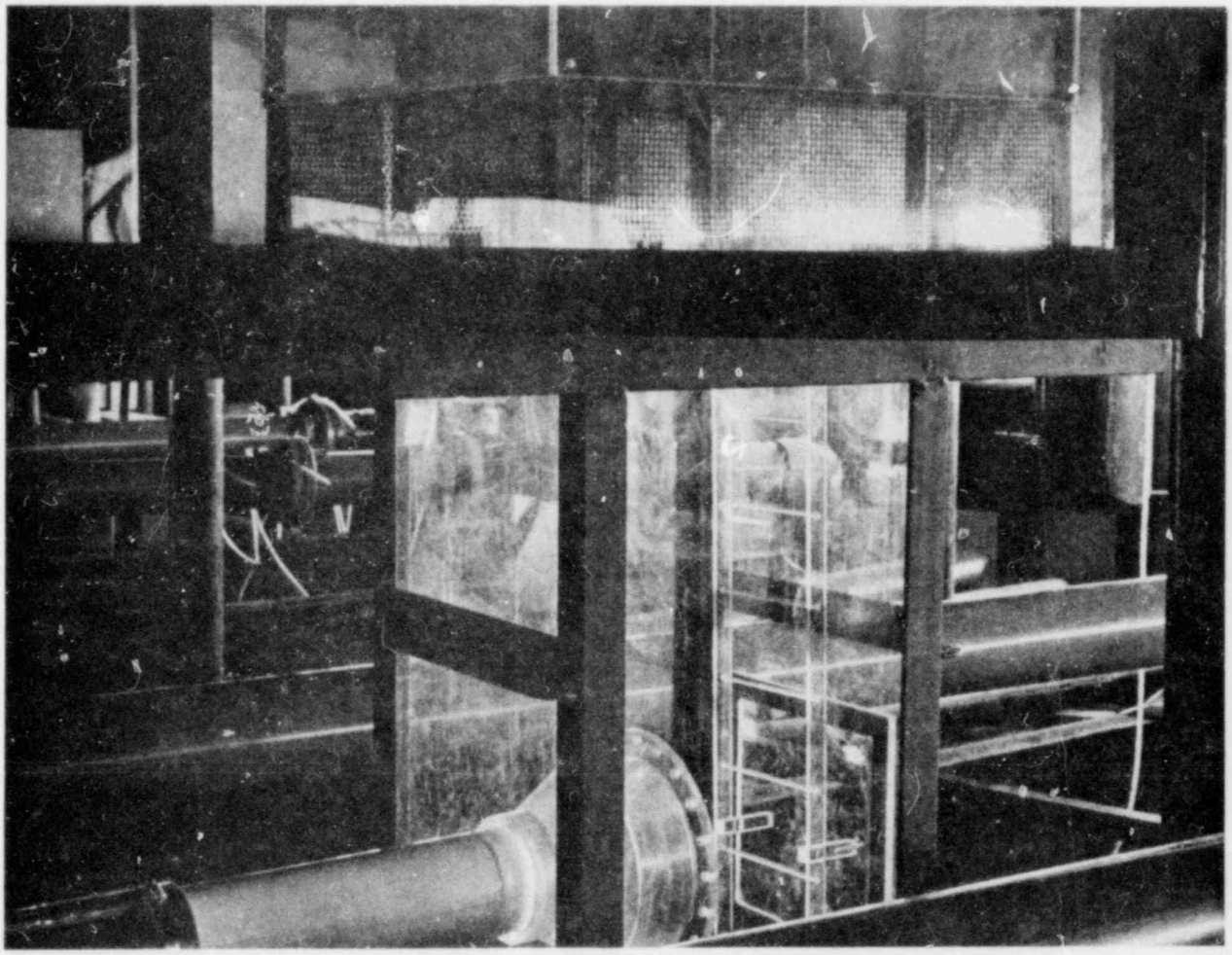

Photograph 4 Model Containment Sump and Pump Sump

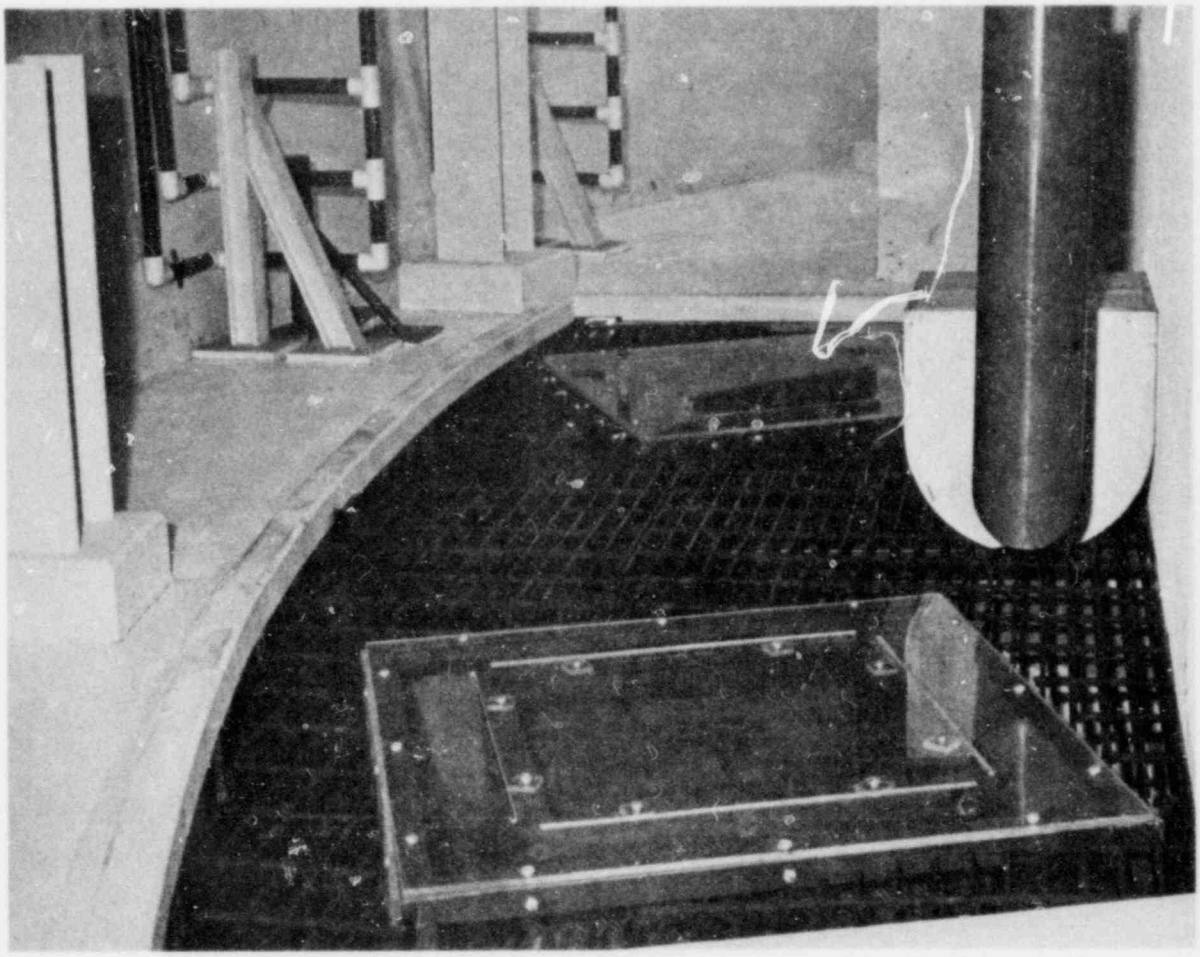

Photograph 5 West Sump – Model

Photograph 6 Southwest Sump – Model

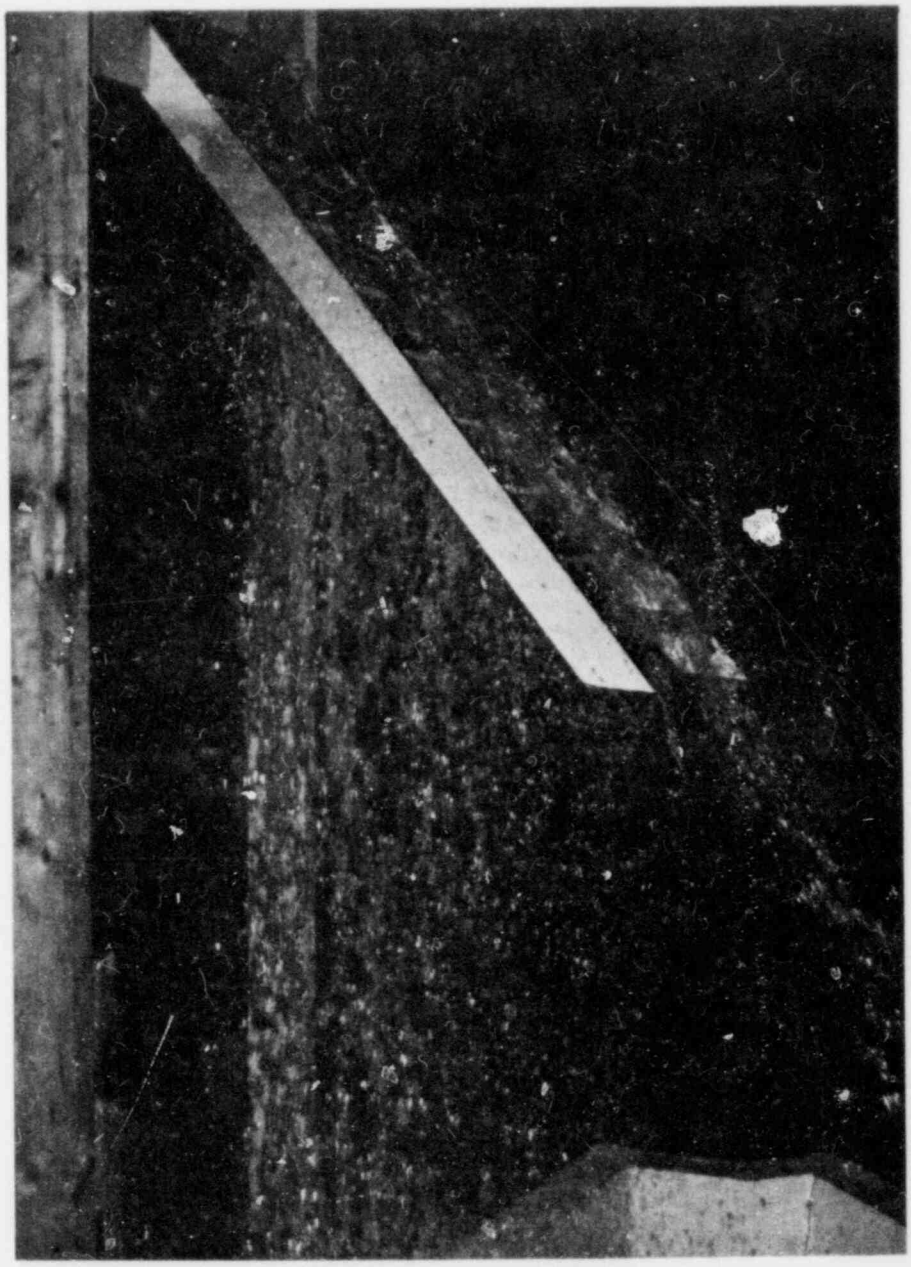

Photograph 7 Flow from Mezzanine Floor
Depth = 6 inches, Flowrate = 1300 gpm

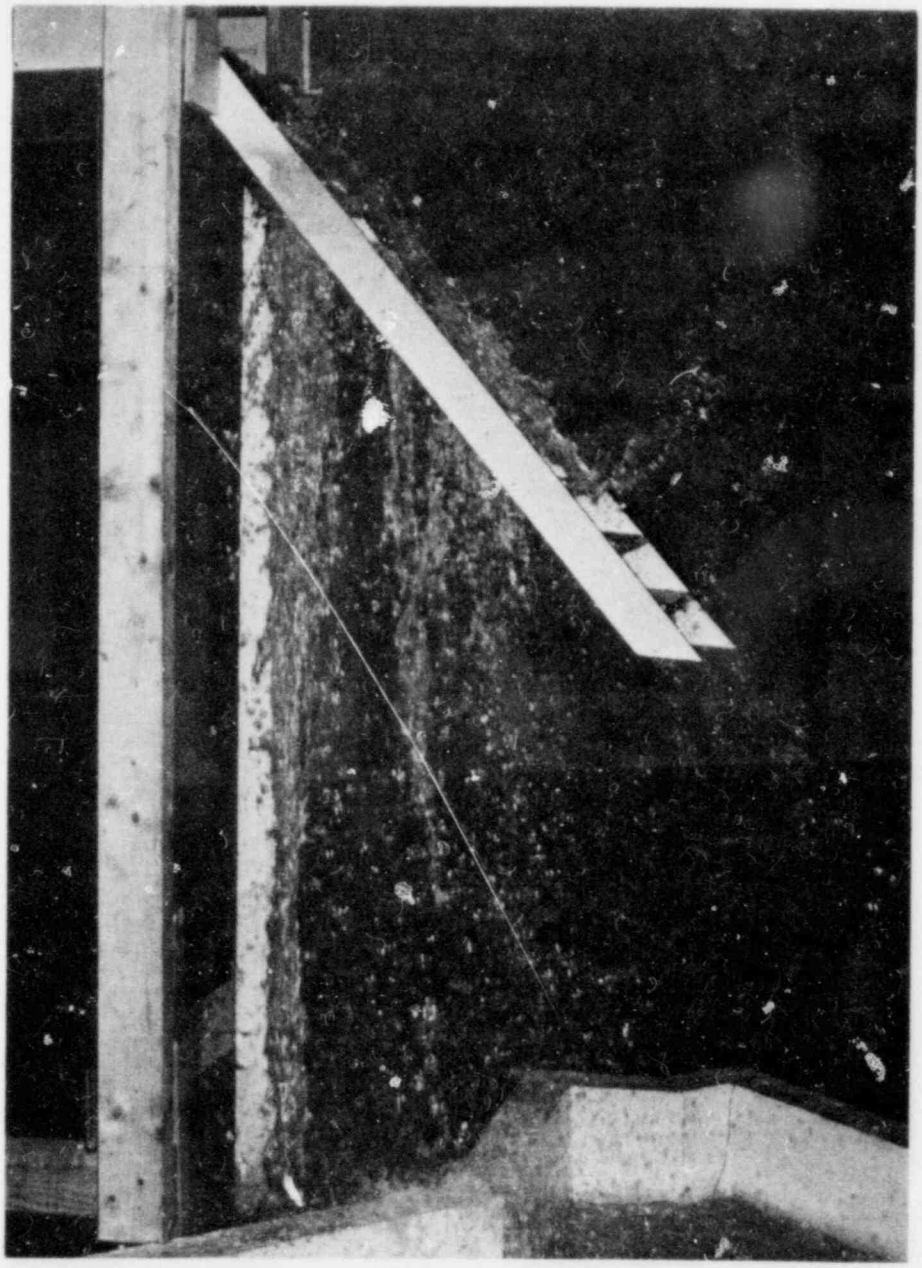

Photograph 8 Flow from Mezzanine Floor
Depth = 5 inches, Flowrate = 990 gpm

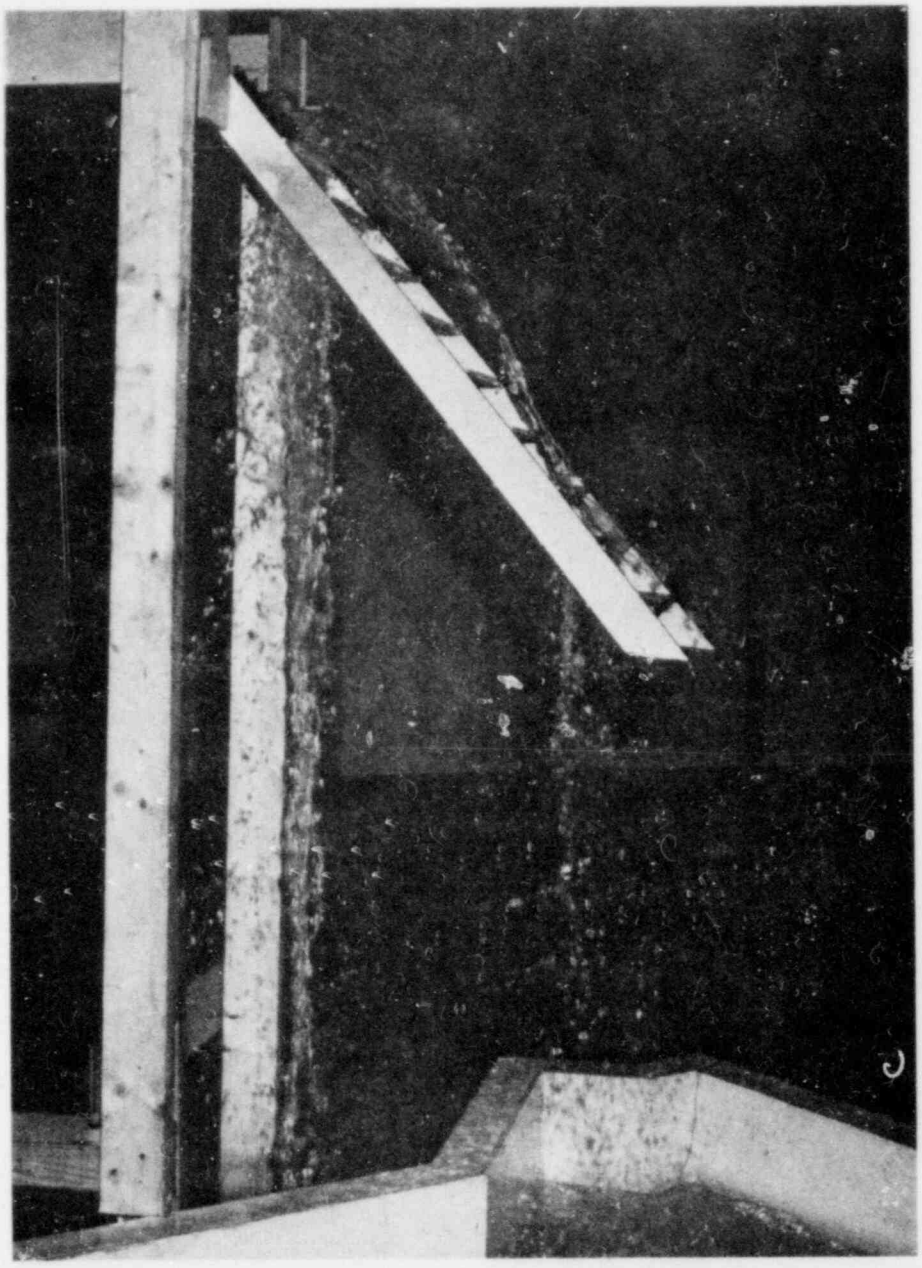

Photograph 9 Flow from Mezzanine Floor
Depth = 4 inches, Flowrate = 680 gpm

APPENDIX A

APPENDIX A

TEST NUMBER		BLOCKAGE			RHR SCREEN LOSS				RB SCREEN LOSS			
F	P	FG	SCREEN	FF	WEST		S W		WEST		S W	
					F	P	F	P	F	P	F	P
1	6	6	0	0	0.068	0.072	0.091	0.038	0.058	0.049	0.106	0.061
2	0	6	0	1	0.043	0.000	0.081	0.000	0.049	0.000	0.042	0.000
3	0	6	0	1	0.043	0.000	0.064	0.000	0.035	0.000	0.044	0.000
4	0	6	0	2	0.026	0.000	0.091	0.000	0.006	0.000	0.048	0.000
5	0	6	0	2	0.040	0.000	0.094	0.000	0.024	0.000	0.059	0.000
6	7	1	0	0	0.000	0.040	0.000	0.098	0.000	0.014	0.000	0.064
7	8	2	0	0	0.000	0.044	0.000	0.067	0.000	0.034	0.000	0.072
8	9	3	0	0	0.000	0.035	0.000	0.060	0.000	0.019	0.000	0.062
9	10	4	0	0	0.000	0.022	0.000	0.076	0.000	0.020	0.000	0.062
10	11	5	0	0	0.000	0.060	0.000	0.061	0.000	0.028	0.000	0.014
11	12	6	0	0	0.000	0.029	0.000	0.083	0.000	0.038	0.000	0.070
12	13	0	1	0	0.000	0.064	0.000	0.092	0.000	0.056	0.000	0.048
13	14	1	2	0	0.000	0.097	0.000	0.186	0.000	0.061	0.000	0.062
14	15	2	3	0	0.000	0.112	0.000	0.153	0.000	0.067	0.000	0.070
15	16	3	4	0	0.000	0.067	0.000	0.104	0.000	0.039	0.000	0.036
16	17	4	5	0	0.000	0.085	0.000	0.123	0.000	0.055	0.000	0.039
52	18	5	6	0	0.079	0.080	0.175	0.116	0.035	0.044	0.060	0.055
18	19	1	7	0	0.000	0.070	0.000	0.076	0.000	0.030	0.000	0.014
19	20	8	8	0	0.000	0.086	0.000	0.107	0.000	0.051	0.000	0.056
33	21	1	8	0	0.081	0.078	0.165	0.145	0.038	0.029	0.063	0.117
37	22	1	8	1	0.078	0.110	0.167	0.073	0.003	0.065	0.110	0.041
38	23	1	8	2	0.067	0.071	0.183	0.091	0.003	0.036	0.118	0.049
53	24	4	8	0	0.089	0.056	0.104	0.098	0.041	0.032	0.027	0.000
34	25	4	8	1	0.102	0.087	0.114	0.082	0.068	0.021	0.057	0.034
35	26	4	8	2	0.000	0.096	0.127	0.116	0.000	0.082	0.054	0.085
32	27	5	8	0	0.066	0.032	0.122	0.110	0.055	0.031	0.038	0.041
31	28	5	8	1	0.097	0.075	0.105	0.101	0.044	0.051	0.077	0.045
30	29	5	8	2	0.090	0.083	0.086	0.096	0.053	0.066	0.031	0.038
56	62	1	2	0	0.084	0.135	0.079	0.118	0.044	0.078	0.053	0.075
57	63	3	2	0	0.073	0.117	0.093	0.127	0.035	0.085	0.047	0.059
58	64	3	2	0	0.089	0.135	0.085	0.117	0.056	0.082	0.027	0.069
39	65	1	4	0	0.085	0.066	0.071	0.070	0.031	0.070	0.015	0.034
40	0	1	4	2	0.093	0.000	0.099	0.000	0.028	0.000	0.065	0.000
41	0	3	4	1	0.064	0.000	0.100	0.000	0.072	0.000	0.009	0.000
42	66	4	4	0	0.082	0.102	0.096	0.095	0.044	0.062	0.059	0.007
43	0	4	4	2	0.101	0.000	0.091	0.000	0.052	0.000	0.059	0.000
44	0	5	4	1	0.075	0.000	0.088	0.000	0.019	0.000	0.039	0.000
45	67	5	4	0	0.059	0.086	0.132	0.115	0.006	0.058	0.035	0.063
46	0	5	4	1	0.090	0.000	0.118	0.000	0.030	0.000	0.048	0.000
47	0	5	4	2	0.093	0.000	0.103	0.000	0.053	0.000	0.074	0.000
55	68	1	6	0	0.079	0.093	0.071	0.075	0.038	0.040	0.036	0.055
0	69	2	6	0	0.000	0.088	0.000	0.069	0.000	0.070	0.000	0.046
0	70	3	6	0	0.000	0.086	0.000	0.810	0.000	0.051	0.000	0.047
54	71	4	6	0	0.073	0.080	0.053	0.074	0.040	0.055	0.024	0.053
0	72	5	6	0	0.000	0.105	0.000	0.103	0.000	0.062	0.000	0.055
50	73	6	6	0	0.077	0.059	0.082	0.076	0.000	0.010	0.043	0.039
48	59	7	4	0	0.081	0.088	0.105	0.087	0.068	0.070	0.050	0.046
49	61	7	4	1	0.097	0.071	0.080	0.101	0.050	0.052	0.036	0.045
60	60	7	4	2	0.070	0.074	0.100	0.100	0.056	0.035	0.024	0.053
51	77	7	6	0	0.075	0.084	0.165	0.109	0.045	0.055	0.106	0.045
0	78	7	6	0	0.000	0.082	0.000	0.076	0.000	0.028	0.000	0.035
0	79	7	2	0	0.000	0.088	0.000	0.143	0.000	0.043	0.000	0.080

NOTE: FLOOR GRATING (FG) AND SCREEN BLOCKAGE CONFIGURATIONS ARE SHOWN IN FIGURES 8 THROUGH 14. APPROACH FLOW DISTRIBUTION (FF), 0 INDICATES NO FLOW STRAIGHTENER BLOCKAGE, 1 INDICATES WEST 50% BLOCKED, AND 2 INDICATES SOUTH 50% BLOCKED.

ARL

APPENDIX B

APPENDIX B

TEST NUMBER		BLOCKAGE			SWIRL ANGLE			
F	P	F.G.	SCREEN	FF	FROUDE		PROTOTYPE	
					RHR	RB	RHR	RB
1	F	0	0	0	-1.9	2.7	-4.3	2.6
2	0	0	0	1	5.0	3.0	0.0	0.0
3	0	0	0	1	-2.6	1.6	0.0	0.0
4	0	0	0	2	4.5	3.3	0.0	0.0
5	0	0	0	2	3.1	1.1	0.0	0.0
6	7	1	0	0	0.0	0.0	-1.3	-2.2
0	8	2	0	0	0.0	0.0	3.2	3.6
0	9	3	0	0	0.0	0.0	1.6	-6.0
0	10	4	0	0	0.0	0.0	-1.1	3.5
0	11	5	0	0	0.0	0.0	-2.6	7.4
0	12	6	0	0	0.0	0.0	-1.4	3.3
0	13	0	1	0	0.0	0.0	7.4	-3.5
0	14	0	2	0	0.0	0.0	4.2	2.4
0	15	0	3	0	0.0	0.0	-9.5	-9.5
0	16	0	4	0	0.0	0.0	2.4	2.3
0	17	0	5	0	0.0	0.0	4.3	2.4
2	18	0	6	0	1.4	1.4	-3.1	-0.4
0	19	0	7	0	0.0	0.0	-2.9	3.2
0	20	0	8	0	0.0	0.0	-4.1	5.4
36	21	1	8	0	3.1	-1.7	-1.6	4.2
37	22	1	8	1	1.1	0.8	1.0	6.1
38	23	1	8	2	1.1	-1.7	-2.5	4.7
39	24	4	8	0	0.7	-2.1	3.5	5.0
34	25	4	8	1	-0.9	-1.1	3.1	5.1
35	26	4	8	2	-1.3	-6.0	2.9	4.7
32	27	6	8	0	5.1	-2.7	4.6	6.0
31	28	6	8	1	5.4	-2.8	4.3	6.8
30	29	6	8	2	4.8	5.5	3.9	7.1
36	62	1	2	0	5.7	3.3	5.0	4.1
37	63	4	2	0	5.0	4.1	3.2	3.
38	64	6	2	0	4.9	2.8	5.0	3.1
39	65	1	4	0	-4.5	-5.5	-2.3	6.1
40	0	1	4	2	-5.0	-6.8	0.0	0.0
41	0	1	4	1	-5.1	-6.3	0.0	0.0
42	66	4	4	0	-5.6	-5.3	-5.1	-6.6
43	0	4	4	2	-5.4	-5.0	0.0	0.0
44	0	4	4	1	-5.1	-5.3	0.0	0.0
45	67	6	4	0	-4.8	-4.1	5.8	5.5
46	0	6	4	1	-5.1	-4.3	0.0	0.0
47	0	6	4	2	-5.5	-4.6	0.0	0.0
33	68	1	6	0	1.4	1.4	1.1	1.5
0	69	2	6	0	0.0	0.0	1.7	1.6
0	70	3	6	0	0.0	0.0	1.8	1.5
34	71	4	6	0	2.4	1.7	2.6	1.6
0	72	5	6	0	0.0	0.0	1.5	2.3
35	73	6	6	0	2.4	1.9	2.0	2.7
48	59	7	4	0	-4.9	-5.8	-5.7	-6.0
49	61	7	4	1	-5.7	-3.9	-6.2	-4.9
50	60	7	4	2	-6.0	-4.4	-5.7	-4.9
51	77	7	6	0	4.7	2.7	2.6	2.2
0	78	7	6	0	0.0	0.0	-1.5	5.4
0	79	7	2	0	0.0	0.0	5.3	4.7
AVERAGE SWIRL ANGLES					3.9	3.4	3.4	4.2

NOTE: FLOOR GRATING (FG) AND SCREEN BLOCKAGE CONFIGURATIONS ARE SHOWN IN FIGURES 8 THROUGH 14. APPROACH FLOW DISTRIBUTION (FF), 0 INDICATES NO FLOW STRAIGHTENER BLOCKAGE, 1 INDICATES WEST 50% BLOCKED, AND 2 INDICATES SOUTH 50% BLOCKED.

ARL

WORCESTER
POLYTECHNIC
INSTITUTE

ALDEN RESEARCH LABORATORY
HOLDEN, MASSACHUSETTS 01520